

POLITECNICO DI TORINO

III Department Information Engineering
Master in Nanotechnologies for ICTs

Master Thesis

Laser Induced Graphene

Implementation and optimization process as supercapacitor
electrode material



Supervisor(s):

Dr. Andrea Lamberti
Prof. Dr. Stefano Passerini,
Co-Supervisor

Candidate name:

DANIELE DI GIOVANNI

July, 2018

Declaration

I hereby declare that, the contents and organization of this dissertation constitute my own original work and does not compromise in any way the rights of third parties, including those relating to the security of personal data.

DANIELE DI GIOVANNI

July, 2018

*I would like to dedicate this thesis to my loving family, they always believed in me
even when I did not.*

*To my friends, my colleagues, to everyone joined me through this path. To the ones I
can share beautiful memories, stories and laughs with.*

To my lovely girlfriend, by my side since four wonderful years.

For all of you, because I could not have been myself without you.

Abstract

The growing energy demand worldwide is pushing researchers for always innovative and better energy storage solutions; among the many and different kind of devices which can collect, store and release energy in form of electrical current, a particular place is occupied by supercapacitors.

An electrochemical capacitor or supercapacitor, is a relatively new energy storage device which shows an intermediate behaviour between a capacitor and a battery in terms of energy and power densities. The typical capacitor plate structure is substituted by a complex nanostructured pattern which allows to hugely increase the active surface while keeping low the volume occupied from the electrodes; this new structure accumulates ions which move in an electrolyte, while in a common capacitor just charges accumulate between plate and insulator. The combination of these two factors generates a far superior charge storage, which seems to have the potential to overcome some of the intrinsic limitations of batteries in the energetic field: low power density, problems at high temperatures and relatively low cycle stability.

Carbon-based materials are a common choice for electrodes, they have large surface area and a well known production process; ions will accumulate on the electrodes surface in response to a superimposed potential to neutralize it, forming a double layer of opposite charges which gives name to the energy storage mechanism, *Electrical Double Layer*. Some carbonaceous materials like graphene gained special interest, because of superior mechanical and conductive properties. In particular Laser Induced Graphene is raising among the possible electrode material in the last decade, due an outstanding ease of production and low costs; LIG is not really graphene, it's graphene-like: a few-layer graphene 3D network, which resembles the original but lacks the long range lattice order. It is also referred as pseudo or amorphous graphene.

The project of this thesis is to carry on a deep analysis of this innovative material, which has potential for flexible electronics, as electrode for a supercapacitor; the analysis will implement an ionic liquid as electrolyte, which grants the device an operating potential window of 3V, three times respect to an aqueous electrolyte supercapacitor.

Three different LIG morphologies obtained by varying laser parameters are compared, so that the best one can be subject of further research for optimization processes. The Needle morphology proves to be unquestionably better than Sheet or Porous, both from the mechanical and the electrochemical point of view; the optimization step regarding the line pattern shows a negligible influence of the line design and interline distance overall. Two different strategies were attempted for LIG doping, a Nitric Acid treatment and a conductive polymer coating with PEDOT:PSS; for contact enhancement instead, platinum was sputtered on top of the LIG area to contact with the aluminum current collector. All of these processes did not seem to produce such a major improvement such as to justify any additional step, which adds more complexity to the production system. On the other side, the flexible device not only does work properly under bending stress, but also seems to have a noticeable upgrade in terms of capacity retain as current density increases.

Laser induced graphenization has presented a strong variable component linked to the unpredictable gas evolution, reason for which resistance and capacitance have a range of values more than a precise one. Nonetheless, results suggest a great potential in flexibility optimization, because of the excellent behaviour shown. Laser Induced Graphene proved to be a bendable, binder free and potentially collector free material to implement for energy storage purposes, with a simple production process, reasons for which LIG is put forward as a promising flexible electronics component.

List of Abbreviations

LIG	L aser I nduced G raphene
EDL	E lectrical D ouble L ayer
EDLC	E lectrical D ouble L ayer C apacitor
PC	P seudo C apacitor
IL	I onic L iquids
CAD	C omputer A ided D esign
CV	C yclic V oltammetry
GCD	G alvanostatic C harge D ischarge
EIS	E lectrochemical I mpedance S pectroscopy
DC	D irect C urrent
AC	A lternating C urrent
XRD	X - R ay D iffraction
XPS	X -ray P hotoelectron S pectroscopy
SEM	S canning E lectron M icroscopy
NA	N itric A cid

Contents

List of Figures	ix
1 Introduction	1
1.1 State of the art	3
1.2 Aim of the Study	4
2 Theory & Materials	5
2.1 Supercapacitors	5
2.2 Supercapacitor materials	8
2.2.1 Electrode	8
2.2.2 Packaging	14
2.3 Supercapacitor electrolytes	15
2.3.1 Ionic Liquid	17
3 Experimental Section	20
3.1 LIG writing	21
3.2 Device assembling	22
3.2.1 Contact issues	25
3.2.2 Optimization modifications	28
3.3 Measurement procedure	29
3.3.1 Cyclic Voltammetry	29

3.3.2	Galvanostatic Charge Discharge	31
3.3.3	Electrochemical Impedance Spectroscopy	32
3.4	Additional analysis tools	34
3.4.1	XRD	34
3.4.2	SEM	35
4	Results and Discussion	37
4.1	Operating Voltage	37
4.2	Morphologies Comparison	39
4.3	Line Writing	41
4.3.1	Device Cyclability	43
4.4	Literature Comparison	45
4.5	Optimization Processes	47
4.5.1	Interline Tuning	47
4.5.2	Contact Enhancement	49
4.5.3	LIG Doping	51
4.5.4	Flexible Assembly	54
4.6	Post Mortem Analysis	59
4.6.1	XRD	59
4.6.2	SEM	61
5	Conclusions	62
	References	65

List of Figures

1.1	Simple scheme of some energy storing devices placed on the Ragone plot, [7]	2
2.1	Helmoltz model of the electrical double layer phenomenon, [4] . . .	6
2.2	The two different mechanisms which contribute to charge storage in supercapacitors. ©Tresso Elena	7
2.3	Supercapacitor charge storage mechanisms summary table, [23] . .	8
2.4	Supercapacitor electrode materials summary table, [23]	9
2.5	(a) 3D scheme of LIG fabrication process using an arbitrary pattern to draw a owl, on polyimide substrate (b) SEM image of the LIG owl pattern, in bright contrast respect to the darker and insulating PI substrate, [13]	10
2.6	Laser Induced Graphene on a coconut, [2]	11
2.7	SEM images of LIG produced in different atmospheres. On the bottom left of each image it is shown the appearance of a water droplet on that specific LIG surface, [12]	12
2.8	FESEM images at low (left) and high (right) magnification for the different morphologies, [8]	13
2.9	Comparison of the electrochemical behaviour of the different morphologies in 1 M Na ₂ SO ₄ employing (a) GCD cycles at 1:25 μ A cm ⁻² , (b) CV at 10mV s ⁻¹ . [8]	13
2.10	Typical coin cell, ©IndiaMART website	14
2.11	Typical rolled packaging, [6]	14

2.12	Typical pouch cell	15
2.13	Electrochemical supercapacitors electrolytes classification, [24] . .	16
2.14	Electrochemical supercapacitors electrolytes main features, [24] . .	16
2.15	Ionic liquid classes compositions, [25]	17
2.16	Pyr_{14}^+ chemical formula, [25]	18
2.17	TFSI^- chemical formula, [25]	18
3.1	3D scheme of LIG fabrication process in a interdigitated pattern, [8]	21
3.2	Right - Step 1: LIG placement on the microscope lab glass, over a pouch foil; Left - Step 2: current collectors fixing, using Kapton adhesive tape	23
3.3	Right - Step 3: glass microfiber separator placed over the electrodes and soaked with ionic liquid; Left - Step 4: Ag reference electrode placement	24
3.4	Right - Step 5: contact enhancement application on the contacts exit side, highlighted from the black arrows; Left - Step 6: final result after the vacuum sealing process	25
3.5	Schematic section of the finished device	25
3.6	Original samples of LIG, needle multiline morphology	26
3.7	Silver paste degradation near the positive electrode	27
3.8	Enlarged contact area of the LIG samples second generation	27
3.9	Supercapacitor charging incapability. The screenshot is taken di- rectly from the measuring program. The working electrode voltage is actually the device one, because the measured system had no reference electrode.	28
3.10	Stabilization of a LIG supercapacitor with needle morphology over 50 CV cycles	30
3.11	Current response to a sinusoidal small signal	32

3.12	Electrochemical Impedance Spectroscopy results of some devices. It is possible to notice how the needle morphology has both the highest and the lowest resistance values, making any comparison with optimizations or different morphologies meaningless.	33
3.13	Example of XRD configuration and data plotting, [1]	35
3.14	Secondary electrons collection illustration, [1]	36
4.1	Devices parameters behaviour with increasing potential window . .	38
4.2	Cyclic Voltammeteries comparison, each morphology CV last cycle .	39
4.3	Capacitance and Efficiency behaviour over increasing current density, at 10, 20, 50 and 100 $\mu\text{A}/\text{cm}^2$	40
4.4	Ragone plots for needle, sheet and porous morphologies	41
4.5	Monoline LIG pattern	42
4.6	Double line LIG pattern	42
4.7	C_s vs Current Density and Ragone plot comparisons for the two line configurations.	43
4.8	Single line LIG C_s and Efficiency vs number of cycles	43
4.9	Double line LIG C_s and Efficiency vs number of cycles	44
4.10	Galvanostatic charge-discharge comparison for the two line configurations, 50 th and 3200 th	45
4.11	Specific capacitance: the LIG results with Pyr ₁₄ TFSI compared Tour research group results implementing BMIM-BF ₄ at discharge current densities from 0.1 mA/cm ⁻² to 7 mA/cm ⁻² , [13]	46
4.12	Ragone plot: LIG results with Pyr ₁₄ TFSI compared to Tour research group data for energy storage devices, [13]	47
4.13	Specific capacitance comparison for different interline values	48
4.14	Coulombic efficiency comparison for different interline values	48
4.15	Ragone plots for different interline values	49
4.16	LIG supercapacitor specific capacitance and efficiency, with and without platinum sputtering	50

4.17	LIG supercapacitor Ragone plots with and without platinum sputtering	51
4.18	LIG supercapacitor specific EIS, with and without platinum sputtering	51
4.19	Specific capacitance vs currenty density of standard LIG and doped LIG devices	52
4.20	Coulombic efficiency vs currenty density f standard LIG and doped LIG devices	53
4.21	Ragone plots f standard LIG and doped LIG devices	54
4.22	Standard and Flexible supercapacitor C_s vs Current density	55
4.23	Standard and Flexible supercapacitor Coulombic efficiency against increasing Current density	55
4.24	Standard and Flexible supercapacitor Ragone plots, comparison	56
4.25	Cyclic Voltammetry comparison for the same device before, during and after the bending process	57
4.26	Specific capacitance vs J comparison for the two different bending radii	57
4.27	Coulombic efficiency vs J comparison for the two different bending radii	58
4.28	Ragone plots comparison for the two different bending radii	58
4.29	X-Ray Diffraction results for anode, cathode and pristine electrode	60
4.30	SEM Laser Induced Graphene images at different magnification levels	60

Chapter 1

Introduction

The increasing energy demand over the last decade has been subject of deep research, addressed to satisfy the incoming need for superior performances into always smaller devices. Microelectronic development and its expansion in new fields, such as the emerging wearable technology and flexible electronics, require a comparable development of the energy storage miniaturization. Batteries represent nowadays the major power source for miniaturized electronics, nevertheless they lack some characteristics which made them unable to entirely fulfill the needs in certain areas [19]: low power density, resulting in complications trying to achieve high charge/discharge rates; heat generation and Joule heating, leading to fast battery degradation over time and increasing safety risks for portable devices; relatively short cycle life [20].

Electrochemical Capacitors, also known as *Supercapacitors*, represent a growing subject for research, which has the potential to work in synergy with batteries for overcoming their energetic vacancies and even to eventually substitute them in peculiar cases, as they possess an hybrid behavior halfway between capacitors and batteries [4] [20]. Superior power density, long term cycle stability, flexible assembly possibility, opportunity to work in harsh environments due different charge storage mechanism are only few of the characteristics which make them so interesting. They also present higher energy density respect to conventional capacitors, and larger charge storage capability, how it can be seen in the Ragone plot reported in 1.1.

Carbonaceous materials are widely employed for supercapacitors applications, because of their Electric Double Layer behavior which enables them to perform at high charge/discharge rate. Carbon based nanomaterials have attractive mechanical

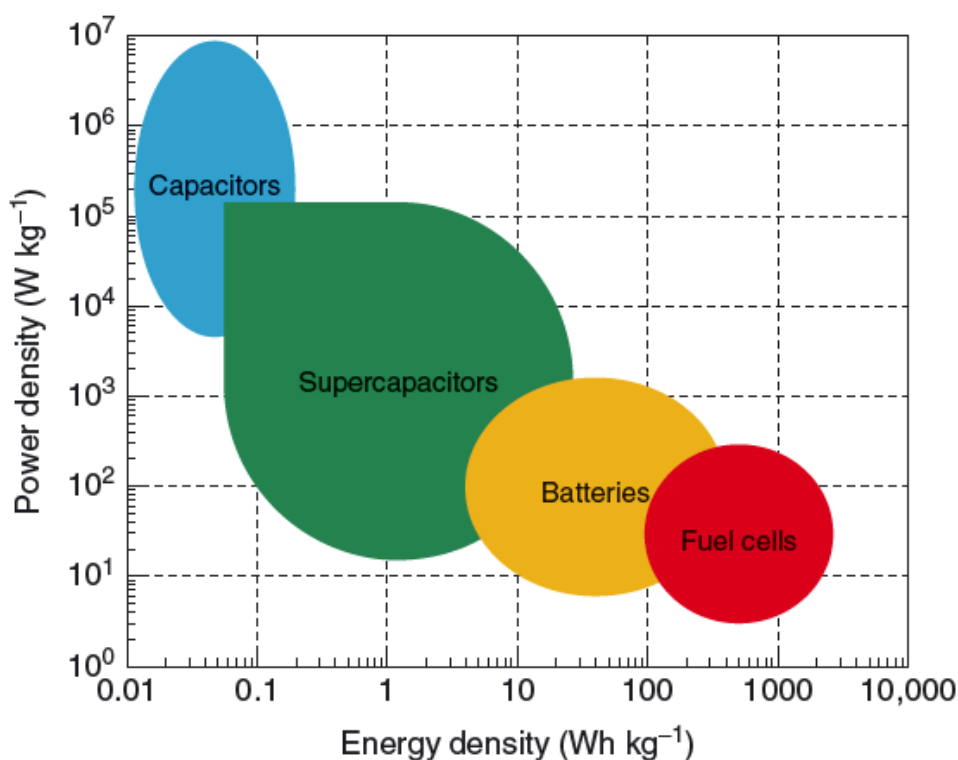


Fig. 1.1 Simple scheme of some energy storing devices placed on the Ragone plot, [7]

and chemical stability, also they can serve both as electroactive material and current collector without the need of a binder [6], which is a great advantage in terms of production simplicity.

Graphene represents a distinguished members of the carbon family, with uncommon two dimensional structure and interesting mechanical properties; it is widely studied nowadays due to its superior conductivity and large surface area, also to more eco-friendly production techniques if compared to other materials. The interest around it is ever growing, as more science fields are studying possible graphene based technology implementations. The curiosity is not restricted to pure graphene though, but to anything which can get close to its singular features, possibly having easier or cheaper production processes. In fact, another class of materials is recently gaining attention because of characteristics which resemble graphene without actually being real graphene, the so called pseudo-graphene materials.

Laser Induced Graphene, also known as LIG, is a graphene-like material produced with single or multiple laser scribing on a surface [2] [21]. Discovered in the 2010s, it is commonly produced on thermoplastic polymers like polyimide and presents an appealing bendability, low cost and ease of manufacture [11] [14], reasons for which it is considered a suitable candidate for flexible electronics applications.

1.1 State of the art

Laser ablation of material and laser employment to obtain graphene are no news in technology, before LIG arrival in 2010s; as matter of fact, direct laser induced reduction of graphene oxide was already used to obtain graphene features [17]. The low cost and ease of production however promptly brought attention to the topic, since the process was further streamlined with simpler and cheaper substrates.

By laser writing it is possible to induce the graphenization of a thin layer on certain materials surfaces, obtaining a porous structure which can be implemented as electrode. Depending on the laser frequency and scan speed, different graphene structures can be obtained, and specific electrochemical characteristics can be found [8].

The classes of materials on whose surface is possible to induce graphenization has enlarged over the years. In the beginning, only a few thermoplastic substrates were reported suitable for this new process [13], in particular polyimide and polyetherimide; research advance has then discovered more substrates possibilities, just new polymers at first [9] and organic materials later as well [21][2]. Common factor between all of them, the determinant that enables the process is the presence of carbon; what has been recently discovered by James Tour research group is that, in fact, any carbon precursor able to be converted in amorphous carbon can therefore be converted in graphene with a multiple lase method [2]. The broad choice of substrates is convenient, not just from a selection standpoint; the possibility of implementing a graphene-like component made with organic and biodegradable material holds a large potential for future technological applications, especially considering that laser can write micrometric patterns.

1.2 Aim of the Study

The purpose of this thesis is to perform a deep analysis of LIG made on Kapton, commercial polyimide, as supercapacitor electrode material; the substrate choice is driven by the well known graphenization process and the possibility to contrast the results with literature. Ionic liquid is chosen to be employed as electrolyte for the purpose of enlarging the window potential respect to a common aqueous electrolyte. This choice will affect energy density, which has a quadratic dependence on the operating voltage [22].

The investigation will initially establish the proper operating voltage, in order to correctly compare the different LIG morphologies one with another without compromising the electrolyte chemistry; once the best performing morphology is chosen, the comparison will focus on the line pattern at first, the optimization process then. The performance improvement attempts will be carried out one by one on the best morphology and will address different aspects: contact enhancement through platinum sputtering, LIG doping with Nitric Acid and PEDOT treatment, flexible device assembly and electrode distance tuning. As last step, a post mortem analysis will be done on a long cycled device, to find out any structure modification and to estimate the performance retain over time.

Chapter 2

Theory & Materials

2.1 Supercapacitors

A Supercapacitor, also named *electrochemical capacitor*, is an high capacitance device that has at least ten times more energy density than a conventional capacitor, and at the same time can also sustain higher current densities and many more charge-discharge cycles respect to a battery. The term "supercapacitor" has been first adopted from the Ottawa group in 1975, for describing the similar behaviour between common and electrochemical capacitors, and the superior capacitance values reached from the latter technology [4].

Compared to normal capacitors, the dielectric material is substituted with an electrolyte in liquid or solid-state form [25], in which charged particles are free to move; the electrodes instead implement nanostructures, so that the active surface area available for charges to gather increases considerably over the volume occupied. In case of liquid electrolytes a supplementary item is required, which is a separator preventing electrodes from touching while still allowing ions movement from one electrode to the other. A solid-state electrolyte separates the two plates by itself, therefore playing a double role in the device structure.

In general, capacitance is defined as the ratio of the electrical charge change respect to the potential change in a given system:

$$C = \frac{\Delta q}{\Delta V} \quad (2.1)$$

It is common to specify a device capacitance value with respect to one of its macroscopic quantity, in order to give a more detailed information regarding the energy storage; the electrode area and weight are two of the most used parameters. The *Specific Capacitance* is widely more used for comparing different storage systems:

$$C_s = \frac{\Delta q}{\Delta V \times \Pi} \quad (2.2)$$

where Π is the macroscopic quantity employed; the measure unit will vary on the characteristic, some recurring ones in electrochemistry are mF/cm^2 and mF/g .

Electrochemical storage in supercapacitors relies on two different types of mechanisms, which may be present singularly or at the same time depending on the material (figure 2.2):

- Electrical Double Layer (EDL) capacitance, an electrostatic process which relies on the Coulomb attraction between opposite charges. Anions and Cations move in antagonistic directions to the two electrodes of the supercapacitor, to neutralize their potential difference externally imposed. Two arrays of opposite charges form facing each other, with high localization and thus high density, a phenomenon referred as Helmholtz double layer model (figure 2.1) ; in this way it is possible to store charge in a relatively fast and highly reversible way. The original preposition of this principle to store electrochemical energy is granted to Backer in 1957 [4], who described in his patent the double layer of porous carbon material perfused with an aqueous electrolyte;

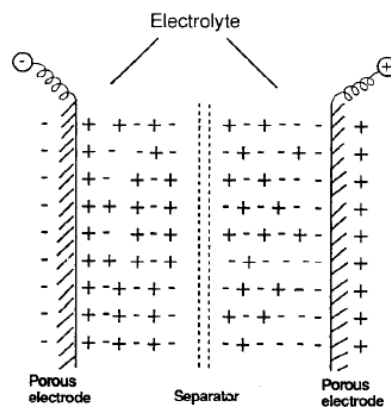


Fig. 2.1 Helmholtz model of the electrical double layer phenomenon, [4]

- Pseudocapacitance, in which Faradaic processes as redox reactions, ion intercalation and electrosorption take place; for thermodynamic reasons, the passed charge q depends on the electrode potential. These processes are reversible and allow the possibility to store a greater amount of charge respect to EDL capacitance; however, the reaction rate limits their speed of usage, and cycle stability over time is not as good. The first record of this charge storage mechanism in a capacitor is attributed to Conway [4], which developed from 1975 to 1981 the electrochemical hydrogen adsorption and electrodeposition of a base metal layer for energy storing.

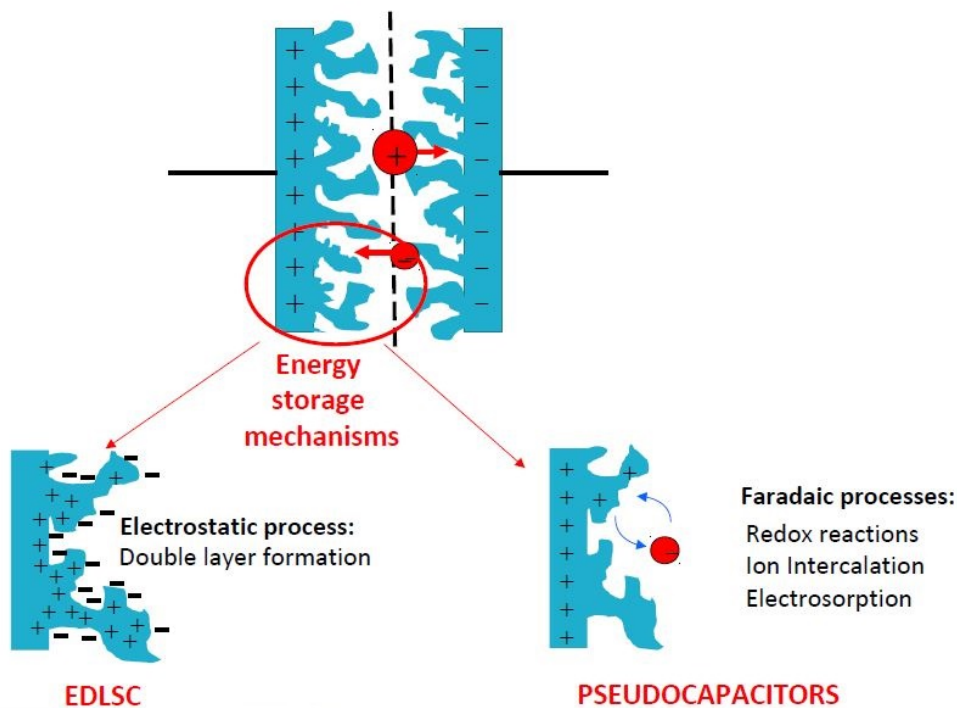


Fig. 2.2 The two different mechanisms which contribute to charge storage in supercapacitors. ©Tresso Elena

The charge storage mechanisms suggest that EDL capacitance involves delocalized electrons from the conduction band, while pseudocapacitance is more a battery-type process and involves valence band electrons [4]. The remarkable lifetime and operating difference is due dissimilar reversibility levels of in the chemical process involved. Faradaic reactions at the anode and cathode interfaces usually imply phase changes of the materials involved; the thermodynamic reversibility can still include partial interconversion irreversibility and material stress which lead to

limited lifetimes. EDL on the other hand has a virtually unlimited cyclability, since no phase change happens during the electrostatic charge transfer, this translates in a much higher but not infinite lifetime, because of inevitable small percentage irreversible components and time degradation of electrodes, electrolyte and packaging. Also, the EDL reaction time constant grants to operate with high charge discharge rates and almost symmetrically. The tab in figure 2.3 briefly resumes the possible mechanisms employable in a supercapacitor.

Type of supercapacitor	Electrode material	Charge storage mechanism	Merits/shortcomings
Electrochemical double layer capacitor (EDLC)	Carbon	Electrochemical double layer (EDL), non-Faradaic process	Good cycling stability, good rate capability, low specific capacitance, low energy density
Pseudocapacitor	Redox metal oxide or redox polymer	Redox reaction, Faradaic process	High specific capacitance, relatively high energy density, relatively high power density, relatively low rate capability
Hybrid capacitor	Asymmetric hybrid	Anode: pseudocapacitance materials, cathode: carbon	High energy density, high power density and good cyclability
	Symmetric composite hybrid	Redox metal oxide/carbon or redox polymer/carbon	High energy density, moderate cost and moderate stability
	Battery-like hybrid	Anode: Li-insertion material, cathode: carbon	High energy density, high cost and requires electrode material capacity match

Fig. 2.3 Supercapacitor charge storage mechanisms summary table, [23]

Supercapacitance characteristics does not allow, at least by now, taking over batteries, except in a few peculiar cases, but rather operating complementary to them in order to fill their performing vacancies.

2.2 Supercapacitor materials

2.2.1 Electrode

The electrode material determines whether the storage mechanism in the supercapacitor will be pseudocapacitive, EDL capacitance or both. This adds more interest about the topic, because a supercapacitor performance can be tuned selecting a given material or two for the purpose of create an EDL supercapacitor, a pseudo-supercapacitor or else an hybrid one, which implements one electrode for each charge storage mechanism [6]. The opportunities are numerous, depending on the desired performance.

There are three main classes of materials which are usually implemented as active electrode material [6]:

- Carbonaceous materials, which are based on the multiple shapes that carbon can acquire. Carbon nanotubes, active carbon composites, graphene and graphene-like structures represent the widest source of choice for electrode material; they are well known and present some desirable advantages from the mechanical point of view. Their charge storage mechanism relies on the EDL, which assures high charge/discharge rates and long cycling life, but the capacitance does not compare to faradaic competitors;
- Conductive polymer materials polyaniline, polypyrrole and polythiophene. Polymers offer an interesting alternative to carbonaceous materials because of their lower cost and superior ease of production. Fast redox reactions allow these materials to be employed as active electrode for pseudocapacitors, whose specific capacitance can reach much higher values compared to the EDL based devices. Nonetheless, the redox phenomena cause more stress in the structure and strongly affects the cycling life;
- Metal oxide based materials such as MnO_2 , RuO_2 and NiO . They exhibit pseudocapacitive behaviour, thus higher specific capacitance compared to carbonaceous materials. However they also have poor power density and low cycle life compared to them because of their storage mechanism, and higher production costs compared to polymers [16]. For this reason they are less employed than the above two classes of materials.

It is also possible to opt for combining two materials, in order achieve superior performances and trying to compensate some material flaws with another one strength. For example, a carbon-based active electrode may be decorated with a pseudocapacitive material to balance out both the specific capacitance and the cycling life [11] [3]. In figure the three material classes and their main characteristics are summarized and compared.

Table 3 Comparison of carbon, metal oxide and metal oxide-carbon composite as supercapacitor electrode

Electrode materials	Surface area	Pore size distribution	Specific capacitance	Conductivity	Rate capability	Stability	Cost
Carbon	High	Various ways to tailor	Low	High	High	Good	Low
Metal oxide	Normally low	Difficult to tailor	High	Low	Low	Poor	High
Metal oxide-carbon composite	Normally controlled by a carbon support	Various ways to tailor depending on the carbon support	High	Tunable, depending on the carbon support	Good	Good	Moderate

Fig. 2.4 Supercapacitor electrode materials summary table, [23]

Laser Induced Graphene

Laser Induced Graphene (LIG) is a rather new subset of carbonaceous materials with some interesting peculiarities which raised the scientific attention about it. A pulsed laser can in fact induce graphenization of certain materials surfaces without completely burning or cutting them. The absorption of proper radiation locally increases the lattice vibrations and raises the temperature over the first layers of material, breaking some atomic bonds; the atoms which undergo this event may rearrange or be released as gas [8]. Atomic rearrangement combined to gas emission produces a porous graphene-like nanostructure with high active area, thus an eligible candidate for supercapacitor active electrode implementation.

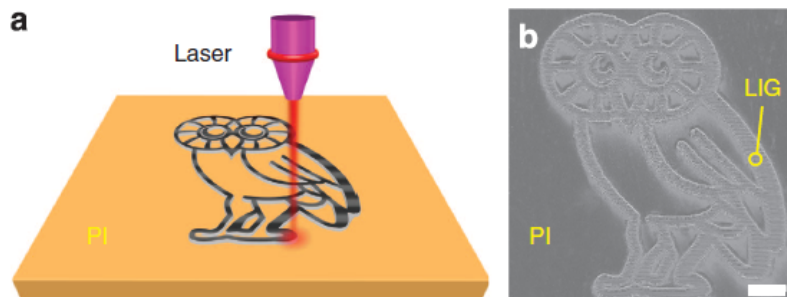


Fig. 2.5 (a) 3D scheme of LIG fabrication process using an arbitrary pattern to draw a owl, on polyimide substrate (b) SEM image of the LIG owl pattern, in bright contrast respect to the darker and insulating PI substrate, [13]

When LIG was introduced in 2010s, only a few thermoplastic polymers like polyimide and polyetherimide were reported available for the graphenization process, and the presence of an aromatic compound was supposed to be the key factor for amorphous graphene formation, with sp^3 carbon atoms being photo-thermally converted to sp^2 hybridization [13]. The list of suitable materials expanded year by year, with other polymers at first [9] and with organic materials then: in 2017 professor James Tour and his research group demonstrated that LIG could be successfully written on wood [21]. Just one year later another paper was published still from the same group, in which it was proved that the aromatic compound was not essential, but in fact any carbon precursor which could be converted into amorphous carbon, was then transformable in amorphous graphene through a multiple lase method (an example is shown in figure 2.6) [2].

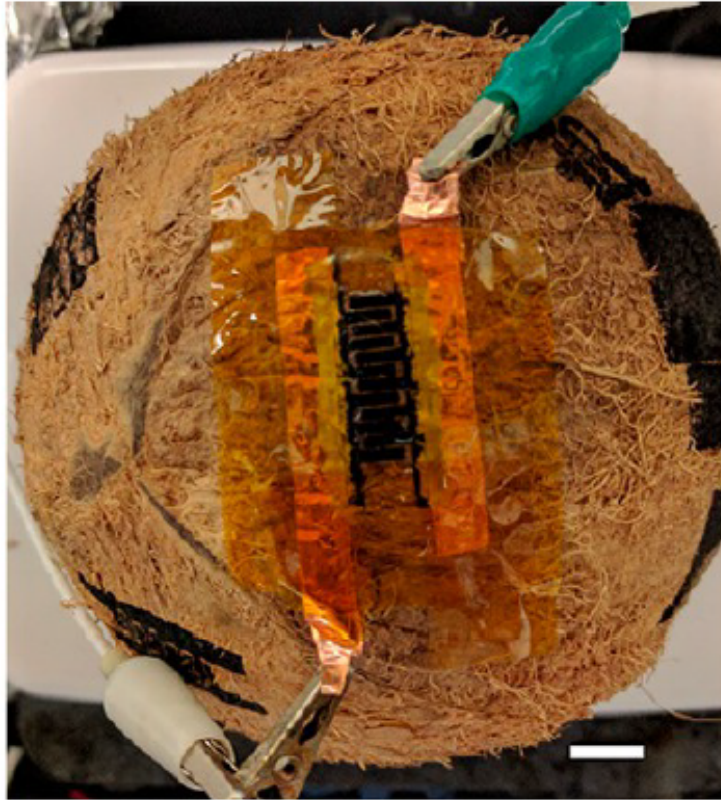


Fig. 2.6 Laser Induced Graphene on a coconut, [2]

Polyimide is the first graphenised material, for this reason a series of studies have been performed since the first LIG production, regarding the effects of laser tuning and controlled atmosphere. The latter study showed a direct link between the selected atmosphere during the LIG writing and the water contact angle, which determines whether the material will be hydrophilic or hydrophobic; oxygen containing atmospheres, as air itself, give the structure superhydrophilic features because of the higher oxygen content and more abundant C-O bonds, which are more polar and water-friendly compared to the C-C and C-H ones. Controlled atmospheres on the other hand, they generate high water contact angle ($> 150^\circ$) and so superhydrophobic features, which may have future application in some peculiar cases [12].

Laser tuning also showed remarkable effects on the system. Dr. Andrea Lamberti and DISAT research group in Turin Polytechnic examined in detail how laser scan speed and frequency influence the gas evolution during the polyimide graphenization process, and so the LIG structure which rearranges differently; three different

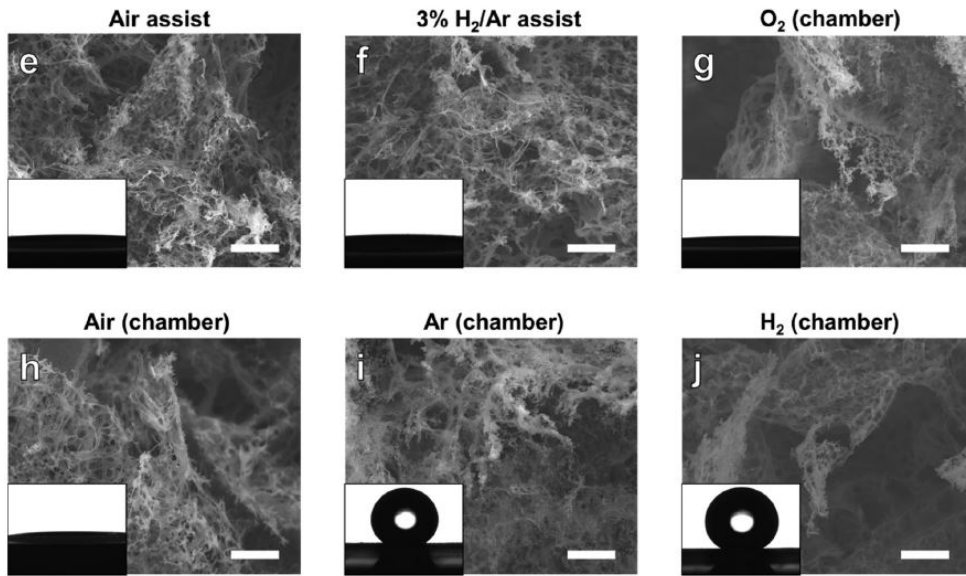


Fig. 2.7 SEM images of LIG produced in different atmospheres. On the bottom left of each image it is shown the appearance of a water droplet on that specific LIG surface, [12]

morphologies have been identified, each one bringing distinct characteristics and conduction properties [8]:

- For 160 mm s^{-1} and 4kHz frequency an elongated structure was obtained, *needle shaped* and almost monodimensional
- Increasing the scan speed to 200 mm s^{-1} the structure changed in a more bidimensional configuration, which resembled a *sheet*
- Lowering the scan speed back to 160 mm s^{-1} and increasing frequency to 20kHz a tridimensional morphology was obtained, in which a submicrometric holes on thin graphene walls formed a *porous* pattern

Porous morphology presented the best graphitic features, with a low amount of C-O functionalities, which should have provided a better behaviour in terms of resistance. However, the structure resulted to be really fragile to handle and easily detachable from the substrate under mechanical stress, while the needle and sheet morphologies resulted more robust and ideally-like behaving during the characterization. One of the reasons is porous morphology lack of nitrogen, because nitrogen defects have proved to enhance capacitance; the precise phenomenon linked to nitrogen beneficial

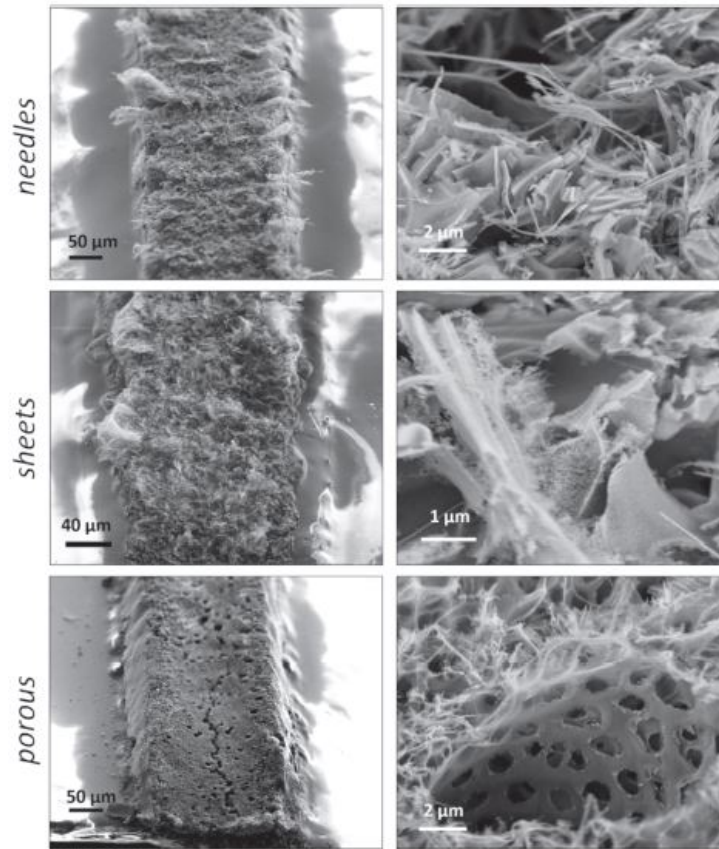


Fig. 2.8 FESEM images at low (left) and high (right) magnification for the different morphologies, [8]

effects has still to be described. Overall, the needle morphology showed the best performance in aqueous electrolyte (1M Na_2SO_4).

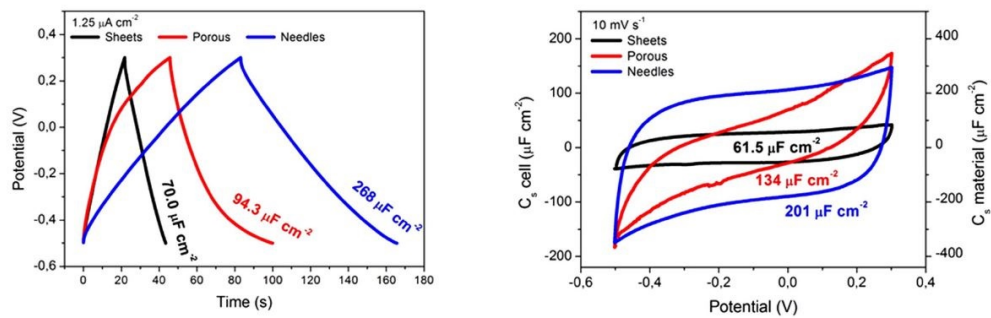


Fig. 2.9 Comparison of the electrochemical behaviour of the different morphologies in 1 M Na_2SO_4 employing (a) GCD cycles at $1.25 \mu A cm^{-2}$, (b) CV at $10 mV s^{-1}$. [8]

2.2.2 Packaging

There are three main packaging methods which are exploited for supercapacitors, which will be briefly described:

- Coin cell, one of the most used and known ones. It assures a robust device sealing, excellent vacuum and low space occupied, nonetheless it requires a contact on the back of the supercapacitor in order to realize any measurement;



Fig. 2.10 Typical coin cell, ©IndiaMART website

- Rolled cell, the most effective one for quantity of material over volume occupied. The device has to be flexible and gets rolled up in a compact structure, this packaging is only available for large areas of active material;

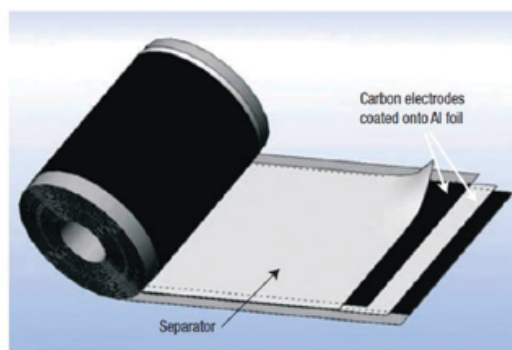


Fig. 2.11 Typical rolled packaging, [6]

- Pouch cell, the most fragile and bulky packaging, but also the most flexible and versatile one for any kind of device. Furthermore, a good vacuum level is assured.

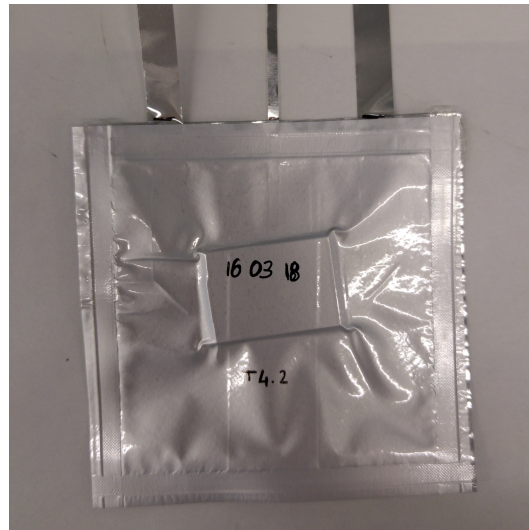


Fig. 2.12 Typical pouch cell

The last option was the one selected for LIG packaging for various reasons: LIG supercapacitor did not have either a back contact or large active material areas; the versatility allowed to make both rigid and flexible devices; the vacuum sealing assured a proper contact between pseudo-graphene and current collectors.

2.3 Supercapacitor electrolytes

The electrolyte choice is important as the electrode material. In fact, the features change from type to type and it is important to take into account various characteristics in order to properly choose accordingly to the designed device. In figures 2.13 and 2.14 are respectively displayed a schematic classification of supercapacitors electrolytes and their main features.

Ionic Liquids were selected to perform the LIG analysis, in order to obtain a wide and stable potential window and to maximize the energy density.

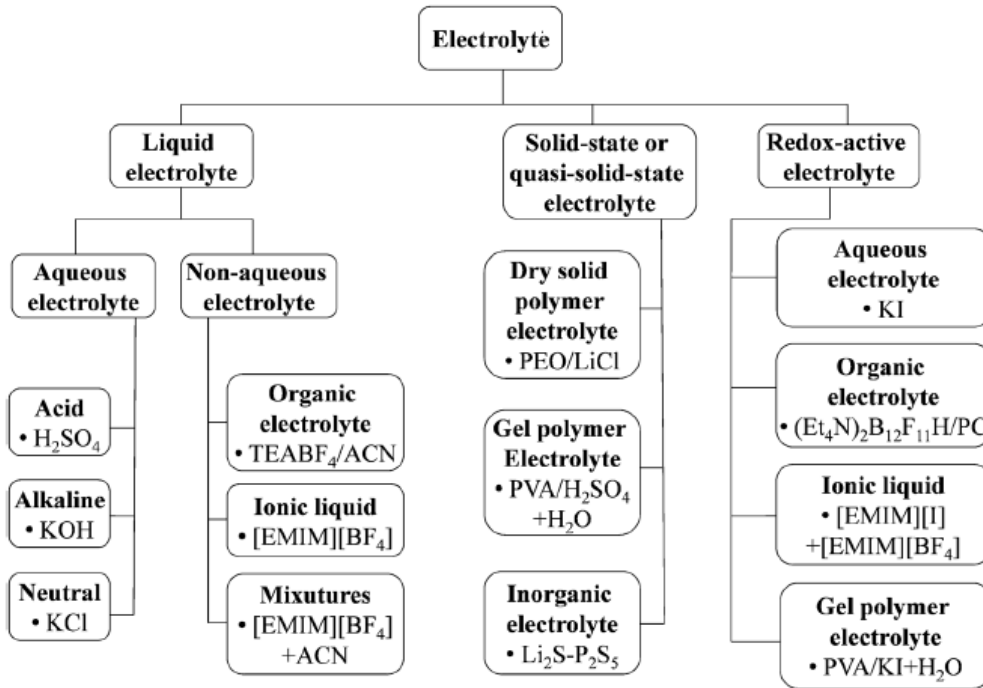


Fig. 2.13 Electrochemical supercapacitors electrolytes classification, [24]

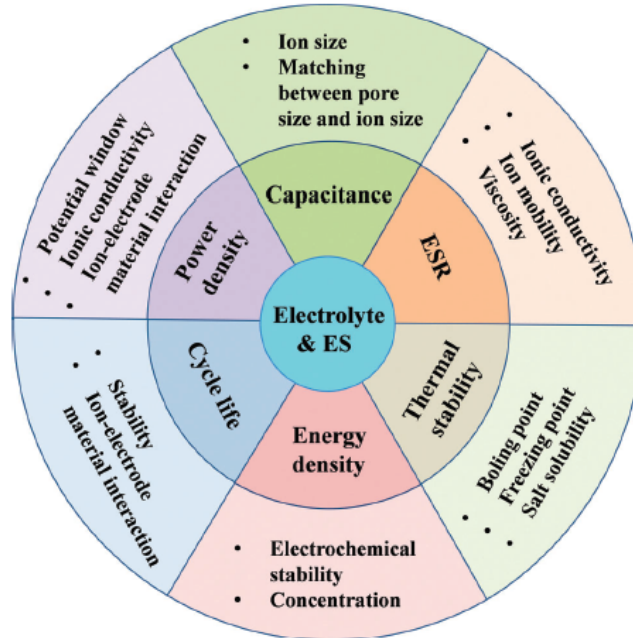


Fig. 2.14 Electrochemical supercapacitors electrolytes main features, [24]

2.3.1 Ionic Liquid

Ionic liquids are salts only made of ions, that have very low melting points, generally under 100°C; for this reason they are also named *low-temperature molten salts*. This peculiar characteristic is provided by the special ions combination, since the cation is usually large, organic and asymmetric, while the anion can be either inorganic or organic. ILs recently drew attention as electrolyte for a supercapacitor because of potential advantages offered by their characteristics [25]:

- High chemical, electrochemical and thermal stability
- Nonflammable
- Negligible volatility
- High operative cell voltages above 3V coupled to EDL capacitors
- High temperature functioning, since there no organic solvent is present
- Large variety of cation-anion combinations, which means tunable properties

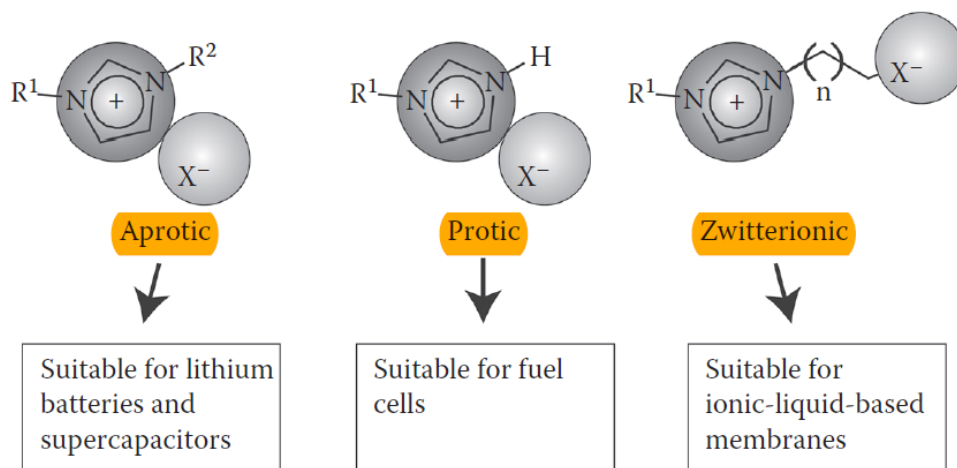


Fig. 2.15 Ionic liquid classes compositions, [25]

As predictable, the set of desirable properties does not come without several disadvantages respect aqueous and organic electrolytes [25]. ILs viscosity is high and ionic conductivity low, so that EDL capacitors exhibit a lower specific capacitance values compared to other electrolytes; the production process of a molten salt is

also quite expensive, and due the large ions employed it is necessary to previously consider the electrodes pores dimension, in order to ensure a proper wetting and the maximum available capacitance.

It is possible to classify ILs in aprotic, protic and zwitterionic, depending on the salt molecule composition as shown in picture 2.15.

Pyr₁₄TFSI

1-Butyl-1-methylpyrrolidinium bis(trifluoromethylsulfonyl)imide, molecular formula Pyr₁₄TFSI, is an aprotic ionic liquid used in electrochemistry with supercapacitors. Pyrrolidinium (Pyr) serves as cation, while the anion is bis(trifluoromethylsulfonyl)imide (TFSI); their chemical formulas are shown in figures 2.16 and 2.17.

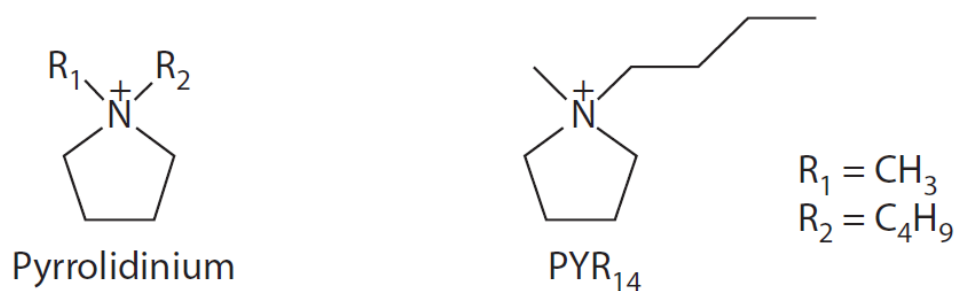


Fig. 2.16 Pyr₁₄⁺ chemical formula, [25]

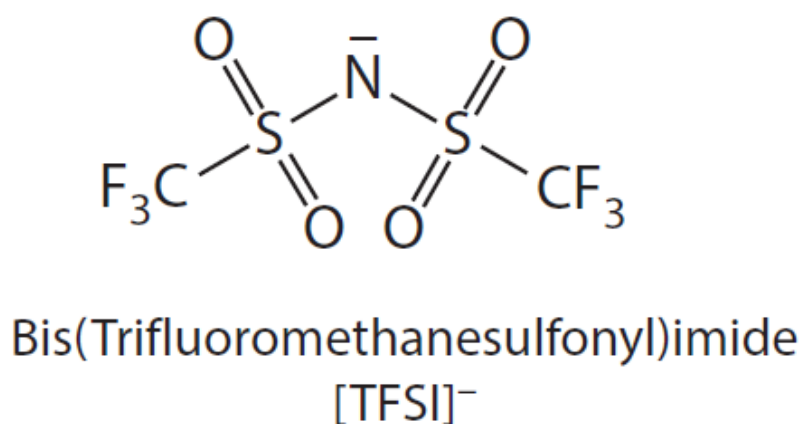


Fig. 2.17 TFSI⁻ chemical formula, [25]

Among the many aprotic liquid suitable for supercapacitor application, Pyr₁₄TFSI is not always the first choice because of its relatively low ionic conductivity which gives a lower capacitance; nonetheless, it has one of the largest electrochemical stable windows in terms of operating voltage and a well known production process, which make it a suitable candidate.

Chapter 3

Experimental Section

The device assembly was entirely performed inside a dry room, in order to prevent any water molecule to get inside the porous LIG matrix and compromise the supercapacitor electrochemical behaviour. The assembly step required this equipment to ensure a precise device sealing in a pouch cell format:

- Pouch cell foil
- Commercial Kapton tape
- Microscope slides
- LIG
- Glass microfiber filters GF/F separator
- N-butyl-N-methylpyrrolidinium bis(trifluoromethanesulfonyl)imide (Pyr₁₄TFSI)
- Aluminum current collectors
- Silver reference electrode
- Adhesion promoter
- Adhesion tape
- Acetone
- Vacuum chamber machine

Once assembled, the supercapacitor performance were evaluated. The entire procedure to assembly a device and measure it will be presented in this chapter.

3.1 LIG writing

The Laser Induced Graphene samples were produced in the MicroLa Optoelectronics laboratories, near Turin, using was a slider CO₂ laser. A schematic representation of the procedure is shown in figure 3.1. The writing process involved one single polyimide piece and one pair of electrodes at time, so as to ensure radiation perpendicularity respect to the target. This guaranteed both the maximum graphenization in depth and the pattern conformity to the CAD design.

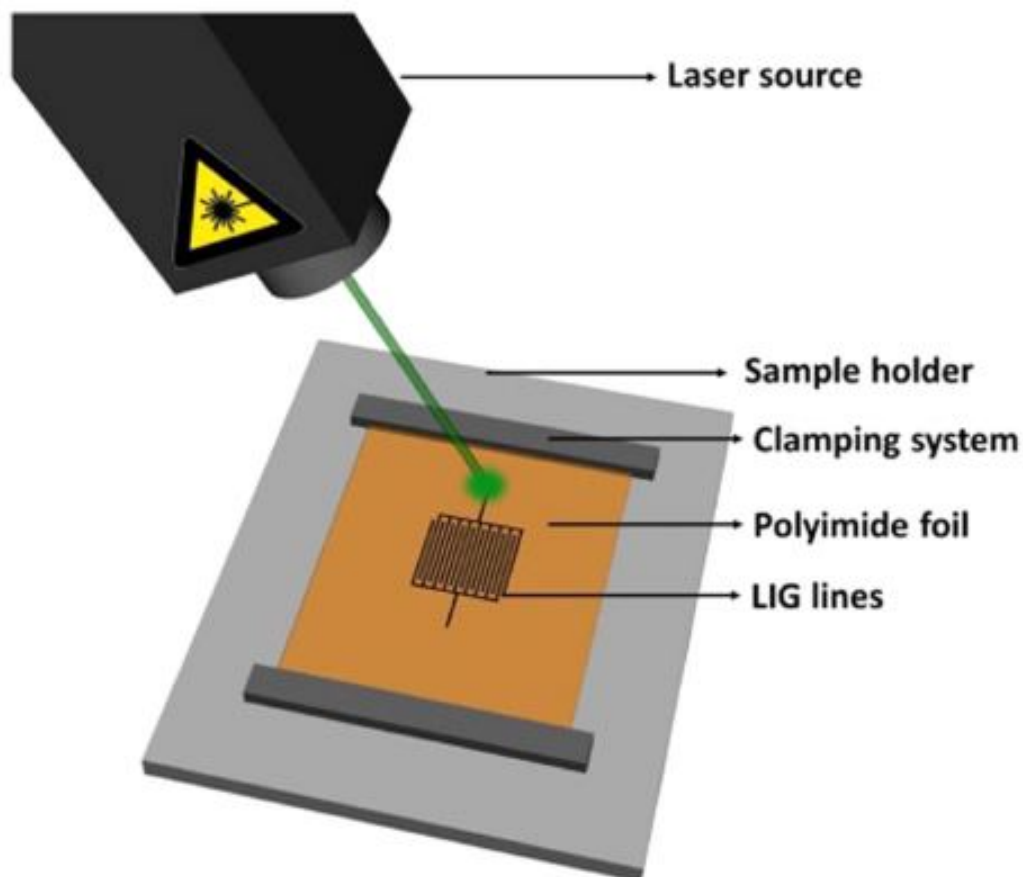


Fig. 3.1 3D scheme of LIG fabrication process in a interdigitated pattern, [8]

The laser parameters employed were the following:

Morphology	Scan Speed	Frequency	Interline	Writing angle	Lasing times
Needle	125 mm/s	4 Hz	no	0°	1
Sheet	200 mm/s	4 Hz	no	0°	1
Porous	150 mm/s	20 Hz	no	0°	1
Porous Area	500 mm/s	20 Hz	170 μm	0° + 90°	2

Furthermore, other two common parameters were also employed:

- Lasing spot, 300 μm
- Lasing power, 2W

These criteria were the result of a previous optimization path for each morphology [8], with the only exception concerning the porous morphology implemented in LIG area: there is no optimization reason behind, but rather those parameters were the result of many attempts. Writing a LIG area with needle or sheet morphology resulted extremely problematic, due the high probability to damage the sample during the lasing process.

The graphenization of an entire area was an important tool to exploit, and has in fact allowed to overcome one of the biggest issues encountered in the project, that is the contact between the LIG electrodes and the Aluminum current collectors. Making a proper contact among them has been a crucial step, which granted the possibility to standardise once for all the procedures of assembly and measurement of the supercapacitors. In fact, LIG irregular and spongy structure could not assure a proper contact with Aluminum without enlarging the touching area, as it will be examined in depth during the next section.

3.2 Device assembling

The appropriate evaluation of the devices electrochemical performance required two fundamental features which conditioned the standard assembly procedure:

- Vacuum environment

- Good electrode-collector contact

In order to achieve both, the established procedure consisted in high vacuum sealing of the supercapacitor inside a pouch cell, and placing the device structure sandwiched between two microscope slides to provide additional pressure for the contact between Aluminum and LIG. Also, an adhesion promoter is exploited on the side where the current collectors and the reference electrode exit the pouch structure, to refine the vacuum sealing. Before assembling, both the electrodes and the separator were dried overnight in a vacuum system, respectively at 120°C and 180°C.

The first, trivial steps to assembly the LIG supercapacitor are shown in figure 3.2. Once the LIG sample was fixed to the lab glass and to the pouch foil, the aluminum current collectors were placed on the graphenised areas; Kapton adhesive tape implementation was not strictly mandatory, but it assured the process integrity without having to introduce a new material inside the device.

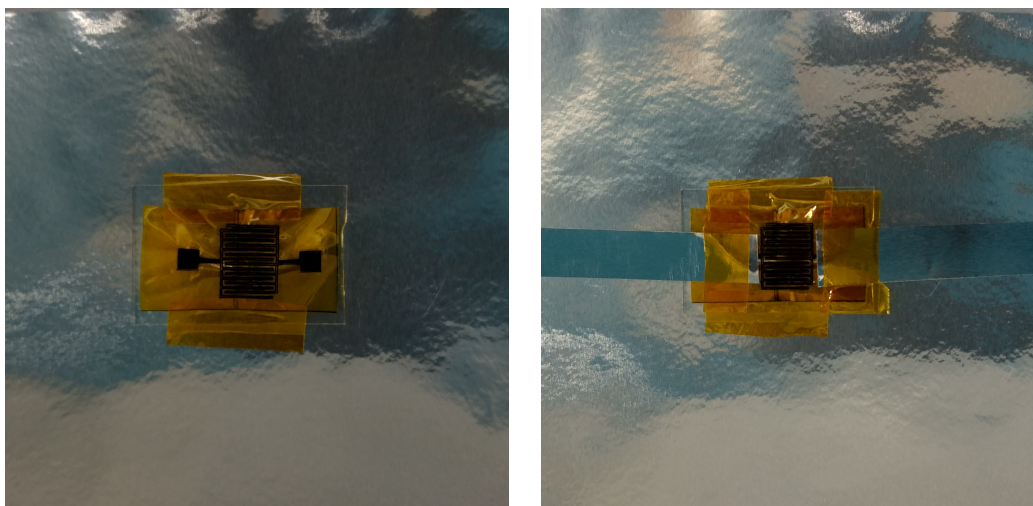


Fig. 3.2 Right - Step 1: LIG placement on the microscope lab glass, over a pouch foil; Left - Step 2: current collectors fixing, using Kapton adhesive tape

The next thing to do was to correctly place the glass microfiber separator, and to drench it with the Pyr₁₄TFSI electrolyte. The reason behind the separator choice lies in the ion movement: the LIG micro-supercapacitor has not a face-to-face system, the electrodes are on the same plane. The ions moving from one electrode to the other first have to raise into the separator first, then move sideways and finally descend; the itinerary required a separator whose ion mobility was isotropic. The implemented separator area was $\sim 4\text{cm}^2$ and for each device a generous quantity of ionic liquid

was used, $\sim 350 - 400\mu\text{L}$. The overabundant Pyr₁₄TFSI assured the devices to perform at the best of their possibilities, both in the first place and in the long run. This last statement is due the voltage range the devices we operated: during the GCD measurements, the working electrode peak voltage raised slightly over the degradation limit, 1.5V vs Ag. Nevertheless, deterioration was negligible thanks to the short "overvoltage" time, compared to a full charge-discharge cycle, and the large quantities of disposable ions in the separator.

The silver reference electrode was then put on top of the wet separator; it consisted of a common aluminum foil sputtered with 50nm of silver on both sides, dried overnight at 120°C with the LIG electrodes. Silver was chosen as pseudo reference electrode, because the implementation of an actual reference was not feasible in such miniaturized device. Furthermore, silver potential is well known from literature and provides sufficient accuracy for the present study. It is important to notice the requirement to make the reference electrode as thin as possible, to ensure the minimum influence on the measurement.

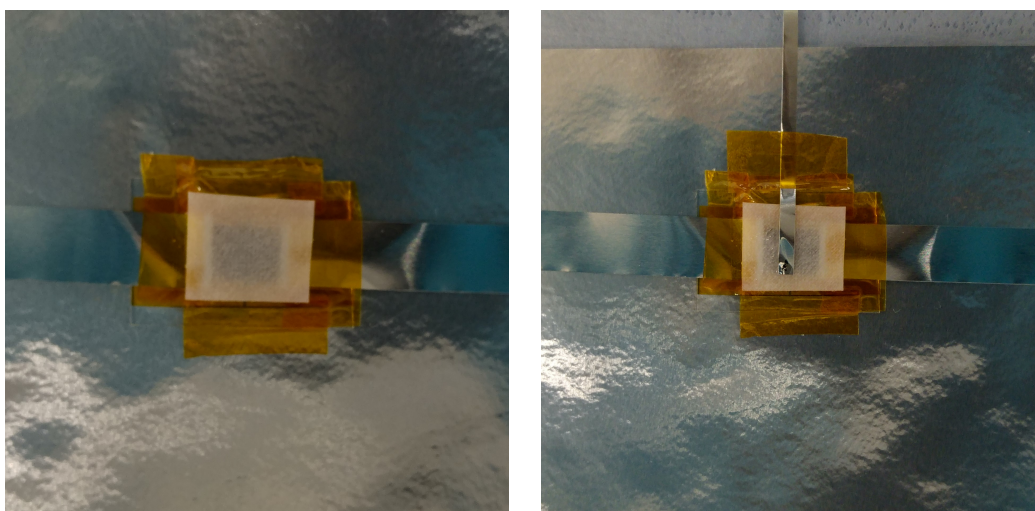


Fig. 3.3 Right - Step 3: glass microfiber separator placed over the electrodes and soaked with ionic liquid; Left - Step 4: Ag reference electrode placement

The last procedure operations rotated around the sealing process. After putting the second microscope lab glass on top of the entire structure, the last matter to deal with was the adhesion enhancement on the pouch foil upper side, from which the aluminum contacts and the reference electrode exit. The adhesion promoter consisted in a special glue coupled with a particular duct tape that were put on both sides respect aluminum and silver, which assured a strong holding and a perfect

sealing also in presence of the two metals. This last assembly part is shown in figure 3.4, while in figure 3.5 a schematic section of the final device is represented.

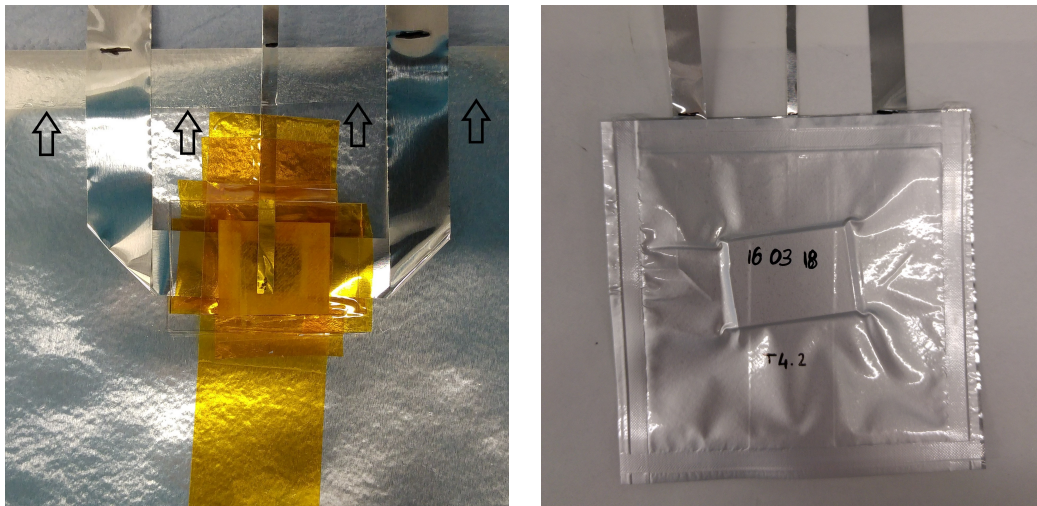


Fig. 3.4 Right - Step 5: contact enhancement application on the contacts exit side, highlighted from the black arrows; Left - Step 6: final result after the vacuum sealing process

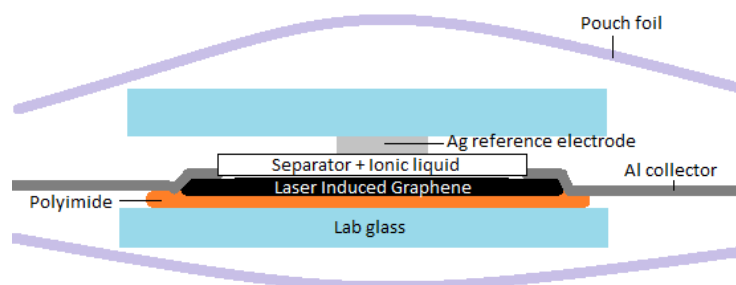


Fig. 3.5 Schematic section of the finished device

3.2.1 Contact issues

The standard procedure was able to assure a satisfying contact, but it was not the first attempt made; the contact realization represented a tricky part in the overall project because of LIG structure itself. The reason has to be found in the small area the first samples provided for the contact, which had the same $\sim 300\text{nm}$ width of electrodes lines (figure 3.6).

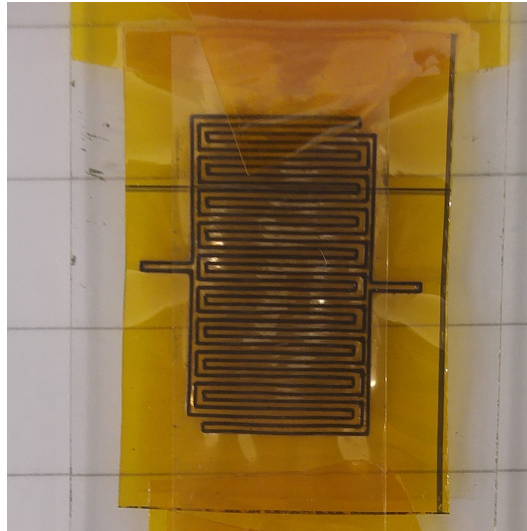


Fig. 3.6 Original samples of LIG, needle multiline morphology

The spongy architecture of the amorphous graphene gave little contact points with the planar aluminum foil, this resulted in a poor current collection and a very resistive behaviour. Two main solution have been tried before finding the right one:

- **Conductive silver paste**

The first solution which came to mind was filling the pores with a conductive paste, which would have enabled a much more simple contact with the aluminum current collector. However, the paste working voltage range was not enough compared to the supercapacitor potential window; the result was a severe paste degradation around the working electrode, probably due the paste polymeric binder degradation and dissolution in the electrolyte. In figure 3.7 is possible to notice the said deterioration.

- **Contact silver sputtering**

In order to overcome the paste degradation problem, the second option sifted through was to sputter a large quantity of silver over the area used for contact, exploiting a proper mask to cover the electrodes; each device had $\sim 100\text{nm}$ Ag sputtered on top. The results given by this resolution were promising but not perfect, the supercapacitors assembled showed variable charge-discharge curves and fluctuating coulombic efficiency for no apparent reason. The hypothesis formulated addressed the fault for this unpredictable behaviour to the small contact area, suggesting that with a larger area would have fixed

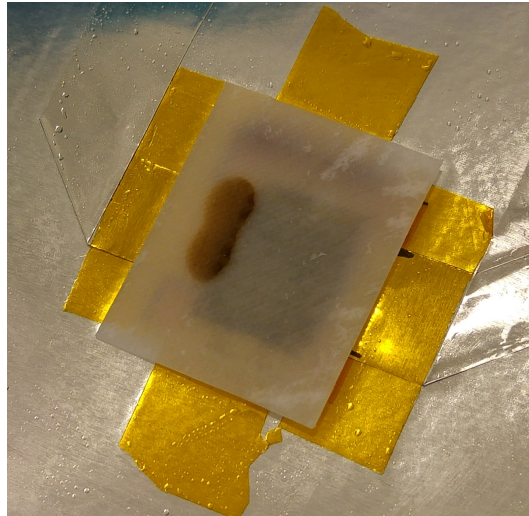


Fig. 3.7 Silver paste degradation near the positive electrode

permanently the problem. For this reason the second generation of samples implemented a much bigger contact area, namely a 5x5mm LIG square plus a 2x5mm connection line to the electrodes (figure 3.8), sputtered as before with 100nm of silver.

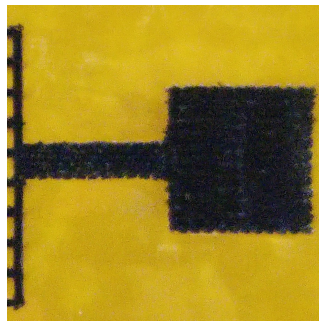


Fig. 3.8 Enlarged contact area of the LIG samples second generation

However the results were even worsened. The supercapacitors could not work anymore in the previous voltage range, and the voltage profile evolved into a faradaic behaviour with a plateau at ca. 0.8 V, suggesting parasitic reaction occurring. The said behaviour is shown in figure 3.9.

A total analysis was performed over any aspect of the assembly process, including LIG morphology and Pyr₁₄TFSI eventual water content. What was discovered, is that the silver itself was the cause of it, and by simply removing

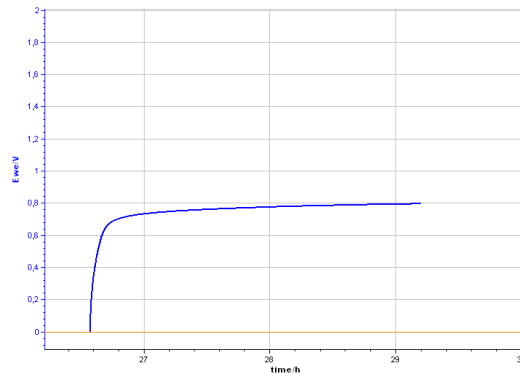


Fig. 3.9 Supercapacitor charging incapability. The screenshot is taken directly from the measuring program. The working electrode voltage is actually the device one, because the measured system had no reference electrode.

the sputtering process the device worked fine. Thus the decision to adopt the last method as the standard one; there was no precise explanation about the silver reaction which justified the abnormal behaviour.

3.2.2 Optimization modifications

The process of supercapacitor production was effective and gave satisfying results, useful for a proper comparison that will be shown later. Nonetheless, a few alterations were made in the last stage, whose goal was to improve the device performance.

- **Interline tuning** - The modification was done not in the assembly process itself, but in the laser writing CAD project, in order to produce devices with a bigger distance from one electrode line to the other;
- **Platinum contact enhancement** - The sputtering stage was added again, but this time a more inert noble metal was exploited, platinum. The reason why it was not attempted before the last stage is merely material: in fact the platinum target for sputtering was not available when the contact issue was faced and dealt with;
- **Bendability** - The lab glasses were removed from the process, in order to give the supercapacitor flexibility, and also for testing the performance when bending;

- **Doping** - The LIG samples were submerged for 30 seconds in a commercial nitric acid solution 69.5%wt in deionized water, then dried out in a convection oven for 30 minutes at 60°C. After the first treatment, half of the samples were submerged in a commercial aqueous solution 1%wt of PEDOT:PSS for another 30 seconds, next they were washed with deionized water to remove excesses and dried again in the convection oven for 30 minutes at 60°C

3.3 Measurement procedure

The measurement process of Laser Induced Graphene based supercapacitors was performed with a multichannel potentiostat system by Bio Logic Science Instruments. The performance analysis of Laser Induced Graphene included three of the most used processes for supercapacitor evaluation:

- Cyclic Voltammetry
- Galvanostatic Charge-Discharge
- Electrochemical Impedance Spectroscopy

The latter only had a secondary role in the general evaluation, while the first two represented the core of it. The first round of measurements were necessary to properly choose the potential window in which the devices would have worked, in which then the supercapacitor would have been tested as a standard procedure.

3.3.1 Cyclic Voltammetry

Cyclic Voltammetry testing sweeps linearly the electric potential in a given range [22]; depending on whether the procedure is performed with two or three electrodes, the potential is applied respectively between positive and negative electrodes, or working and reference electrodes. The instantaneous current recorded during the measurement provides informations regarding the electrochemical reactions happening in real time, and whether they are reversible or not; the final curve shape is an evaluation first sight tool which has not to be underestimated. The rate at which the voltage is scanned, the *scan rate* v , represents a key analysis parameter: the higher

scan rate, the lesser time to complete a single cycle, but also the more reactions which will be overlooked. Most of the faradaic reaction in fact take place in relatively long times, so they require slow scan rates to be seen; it is then important to wisely choose v , accordingly to each own requirements.

EDL capacitors are expected to have a CV plot current vs voltage with a rather rectangular plot, while pseudocapacitors exhibit some peaks associated to reversible redox [22]; the scan rate influences proportionally the EDL capacitors whereas in pseudocapacitance current proportionality is only proportional to the square root of it. The difference is significant enough to distinguish properly the two mechanisms one from the other while testing.

The Cyclic Voltammetry was the starting point of the supercapacitor analysis. Final goal of this first operation was to initialize the device, forcing the voltage window to help ion movement and intercalation in the porous structure; CVs were performed with only two electrodes without connecting any reference, so that $V_{we}-V_{ce}$ was controlled, not just the working electrode potential. The scan speed adopted was 10mV/s and the number of cycles fixed to 50, since the carbonaceous composition of the electrode material did not really require a long time to reach a stable behaviour, as shown in picture 3.10. The first cycles peaks were associated to material impurities non reversible reactions, hypothesis reinforced by their fast disappearing over time.

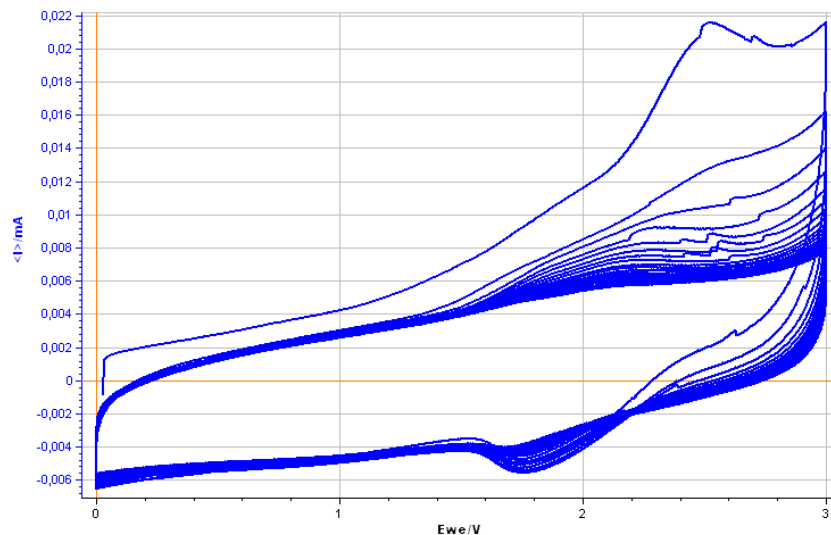


Fig. 3.10 Stabilization of a LIG supercapacitor with needle morphology over 50 CV cycles

3.3.2 Galvanostatic Charge Discharge

Galvanostatic Charge Discharge, or Constant Current Charge Discharge, is the most employed method for supercapacitor characterization; the device is repetitively charged and discharged to given voltage values, using a constant current level. The current level choice is then fundamental, in order to produce comparable data. Other than core parameters, the GCD can be exploited to test the device cycling stability and performance over time, and for this reason is still reputed the most convenient and accurate testing approach [22].

The Galvanostatic Charge Discharge measurement allowed to extract most of the informations regarding Laser Induced Graphene supercapacitors. The first measurement, aimed to determine the optimal potential window, used a constant $10\mu A/cm^2$ density of current; when the maximum operating voltage was established, multiple values of J were employed to investigate the performance in terms of power and energy density, namely 10, 20, 50 and $100\mu A/cm^2$. In particular, the main characteristics employed to compare the different morphologies and configurations were four; they are listed below, associated to the respective formula to calculate them. [22] [11]:

- Specific capacitance (mF/cm²)

$$C_s = \frac{I \times t}{Area \times 3600 \times \Delta V} = \frac{Q}{Area \times \Delta V} \quad (3.1)$$

- Coulombic efficiency (%)

$$\eta_c = \frac{C_{MAX,discharge}}{C_{MAX,charge}} \times 100 \quad (3.2)$$

- Energy density ($\mu Wh/cm^2$)

$$E_d = \frac{\int^{t_{discharge}} V \times I dt}{3600 \times Area} \times 10^6 \quad (3.3)$$

- Power density ($\mu W/cm^2$)

$$P_d = \frac{E_d \times 3600}{t_{discharge}} \quad (3.4)$$

LEGEND

I = current, mA

t = time, s

Area = electrode graphenised active area, cm^2

V = voltage, V

Q = charge, mAh

 C_{MAX} = maximum capacitance, $\mu\text{F}/\text{cm}^2$

3.3.3 Electrochemical Impedance Spectroscopy

Electrochemical Impedance Spectroscopy, also known as dielectric spectroscopic testing, investigates a device impedance as a function of the frequency. The measure is achieved by superimposition of a DC bias voltage and a sinusoidal small signal in a broad range of frequencies; the AC signal is small so that the system response is pseudo-linear, that means a sinusoidal current with the same frequency and shifted in phase 3.11. The current can then be estimated as a sum of sinusoidal functions through Fourier series [5].

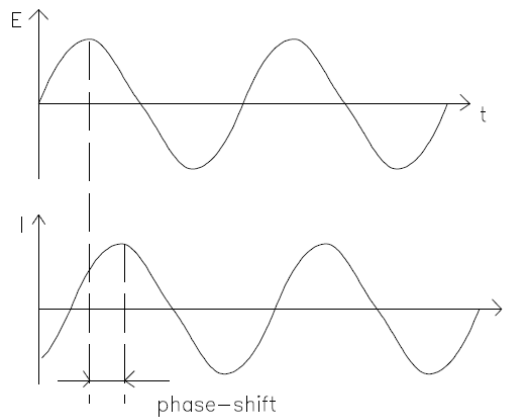


Fig. 3.11 Current response to a sinusoidal small signal

In such system, voltage and current response can be expressed in terms of magnitude and phase shift,

$$V_t = V_0 \exp(j\omega t) \quad (3.5)$$

$$I_t = I_0 \exp(j\omega t - \phi) \quad (3.6)$$

It's therefore possible to write the impedance as a complex number,

$$Z(\omega) = \frac{V}{I} = Z_0 \exp(j\phi) = Z_0(\cos\phi + j\sin\phi) = Z' + jZ'' \quad (3.7)$$

Results are usually reported in a Nyquist plot, in which the real and the imaginary component of Z are displayed respectively on the x and y axis, along with a Bode plot where the phase is shown respect to the frequency. EIS response permits to evaluate charge transfer and charge storage mechanisms, mass transport, estimate capacitance values, equivalent series resistance, energy and power properties. The accuracy of values is yet lower than GCD analysis, for this reason this test was employed only for a qualitative assessment of supercapacitor behaviour.

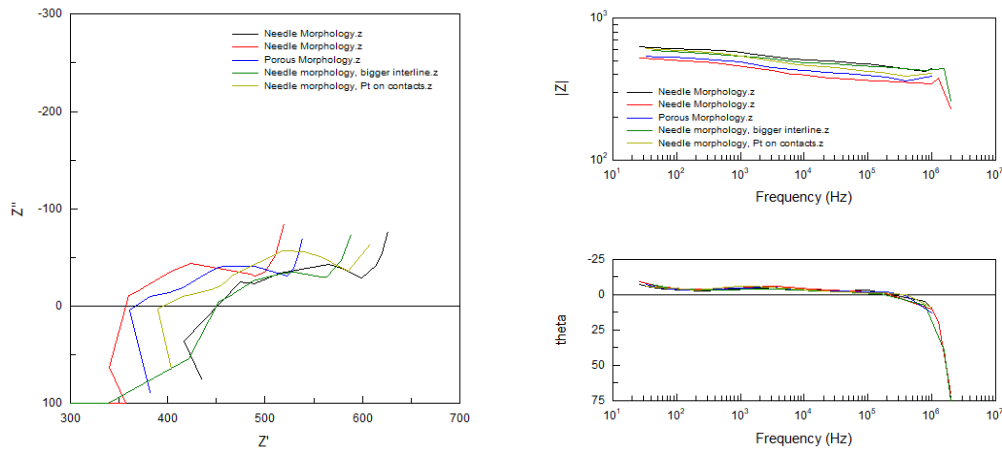


Fig. 3.12 Electrochemical Impedance Spectroscopy results of some devices. It is possible to notice how the needle morphology has both the highest and the lowest resistance values, making any comparison with optimizations or different morphologies meaningless.

The randomness of Laser Induced Graphene production due gas evolution reflected in supercapacitor behaviour: resistance values were not replicable, two devices of the same kind could have completely different R_{ES} values even when assembled in the same day, with LIG samples from the same production stock . The

Nyquist plots were similar one to the other, even unexpected performances were comparable and common to every type of LIG tested. For this reason EIS data could only be employed for a qualitative and superficial analysis, and will not be discussed in the following chapter about results and comparison. Moreover, for the very same reason any formulas including R_{ES} were avoided on purpose, to ensure the impact to be as little as possible on the other device characteristics.

3.4 Additional analysis tools

The supercapacitor electrochemical performance is a fundamental feature, but is not the only one concerning the deep analysis which has been carried out during this project. The elemental composition, the material crystallinity, the pseudo-graphene topography, they all influence the final performance and have therefore to be taken in consideration. This section will cover the supplementary analyses and their intention.

3.4.1 XRD

X-Ray Diffraction data analysis is a characterization technique which allows to acquire information regarding the crystalline structure and unit cell parameters [1].

The sample is placed in a chamber and bombarded with a fixed and properly focused X-ray beam, while a detector rotates around it. The number of X-rays collected at each angle 2θ is recorded, and the intensity is then plotted as function of the rotating angle itself (figure 3.13)

The XRD diffraction pattern is specific for the particular chemistry and atomic arrangement, two materials with different crystalline phase will not produce the same graph. The more ordered structure, the sharper the pattern peaks will be; on the contrary, amorphous materials will produce very low and broad peaks. The XRD allows then to determine the structure crystalline phases, and to inspect any modification of the same: comparing two patterns of the same material it is possible to investigate for any change in the structure given by defects, stress, doping or temperature, for the peaks will change or broaden.

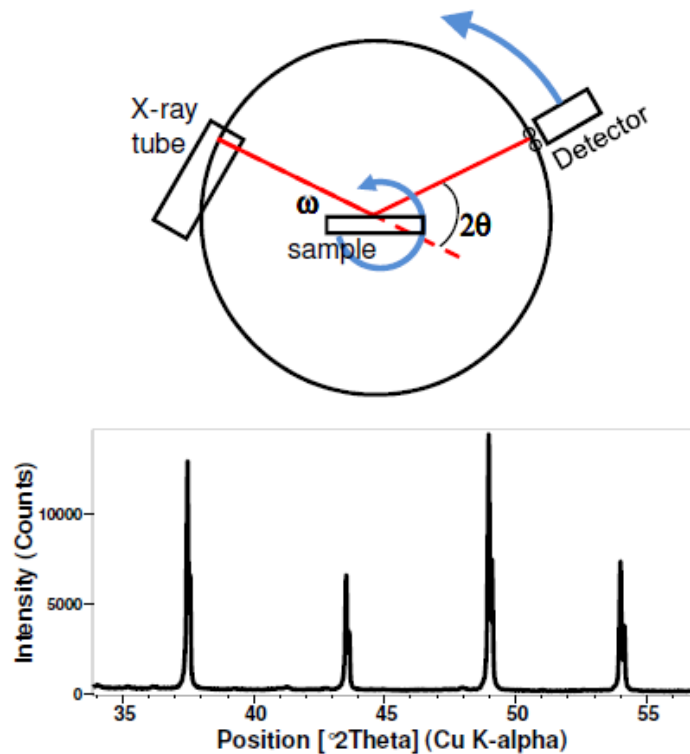


Fig. 3.13 Example of XRD configuration and data plotting, [1]

3.4.2 SEM

Scanning Electron Microscopy is a useful tool to examine micrometric and nanometric elements whose dimension is too small for common optical microscopy. Instead of light, an electron beam is used for the investigation, condensed by electromagnetic lenses and not glass ones [1]. The electron beam causes other electrons detachment from the first layers of the material, also called Secondary Electrons; SE are collected from a detector and their signal amplified, as in figure 3.14.

Secondary electron signals are collected and translated into an image, with a magnification factor which can go up to $\times 300000$, and also with a depth of field 300 times increased respect to light microscopy: the result is a clear 3-dimensional image of the sample superficial topography.

SEM greater inspection resources come with some additional performing requirements, the system needs to operate under vacuum and to interact with a conductive surface, even when the material is not. Because of that, all non-conductive materials

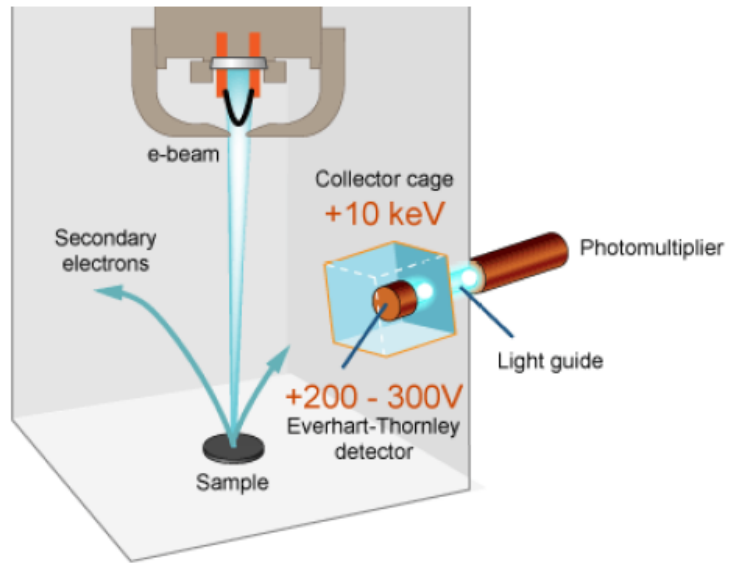


Fig. 3.14 Secondary electrons collection illustration, [1]

require a thin layer of metal to be sputtered, in order to work efficiently; Laser Induced Graphene did not require any sputtering step, since amorphous graphene proved itself to be sufficiently conductive.

Chapter 4

Results and Discussion

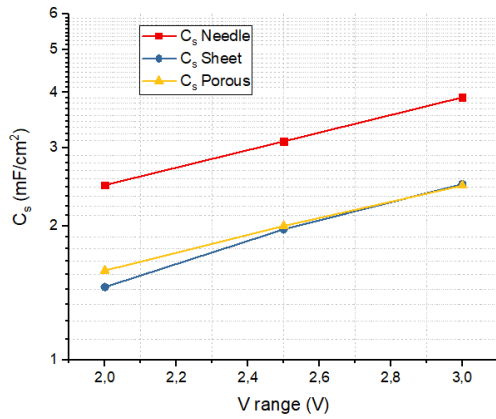
The results obtained from the previously described experimental setup are presented in detail in the following chapter. A proper data analysis and comparison will be performed in each section and finally, conclusions will be drawn about the LIG implementation as supercapacitor electrode material and the potential improvement achievable through an optimization process.

4.1 Operating Voltage

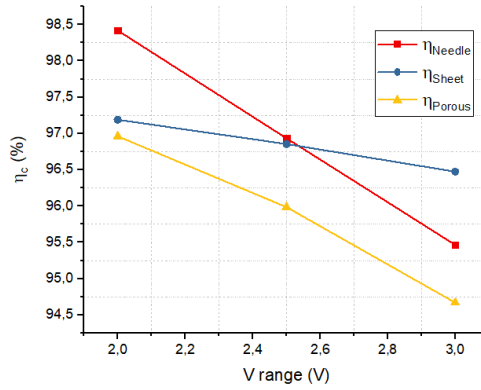
The first operation required by the Laser Induced Graphene analysis, was to establish the proper supercapacitor operating voltage. *Pyr₁₄TFSI* electrochemical stability assured a potential window at least double respect to an aqueous electrolyte, nonetheless other parameters had to be taken in consideration; the galvanostatic measurement highlights eventual dissimilarities between charge and discharge curves as voltage increasing, and this might have undermined device efficiency.

Three supercapacitor were assembled, one per morphology, and initialized with a Cyclic Voltammetry up to 2V; after that each device underwent three GCD measurements. Every GCD had one hundred charge-discharge cycles at $10\mu\text{A}/\text{cm}^2$, while the potential window increased regularly: 2V, 2.5V and 3V.

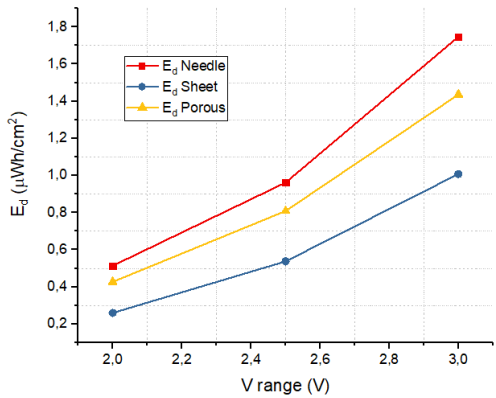
The graphs reported in 4.1 show the three morphologies behaviour with increasing operating voltage. Both specific capacitance and power density had a perfectly linear increase with voltage, while the energy density had a slight increase stepping



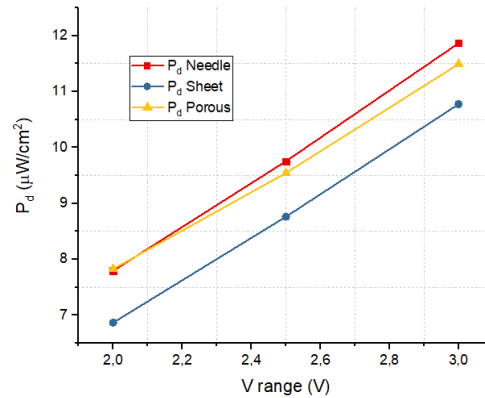
(a) Specific capacitance vs Voltage



(b) Coulombic efficiency vs Voltage



(c) Energy density vs Voltage



(d) Power density vs Voltage

Fig. 4.1 Devices parameters behaviour with increasing potential window

from 2.5V to 3V, pointed out by the different slope (figure 4.1c). For what concerns the coulombic efficiency the expected decrease was present, but was not identical for every morphology: the LIG sheet morphology seemed to suffer less the window enlargement, and its η_c value remained almost constant.

Because of the remarkable boost of C_s , P_d and E_d , 3V was chosen as voltage window for all three morphologies. The efficiency decrease of a few points in percentage has been a downside, but any morphology still kept more than satisfying value while increasing the other parameters; in particular, increasing from 2V to 3V granted multiplying E_d at least by a factor three. The lower ion conductivity of ionic liquids did not allow to reach any power density comparable to aqueous

electrolyte LIG devices [11], so it was decided to extend as much as possible the potential, maximizing the performance in terms of energy density.

4.2 Morphologies Comparison

The morphology comparison was performed with new assembled supercapacitors, preventing any error related to previous devices use; an activation 50 cycles CV was performed sweeping the $V_{WE} - V_{CE}$ to 3V, the established operating voltage.

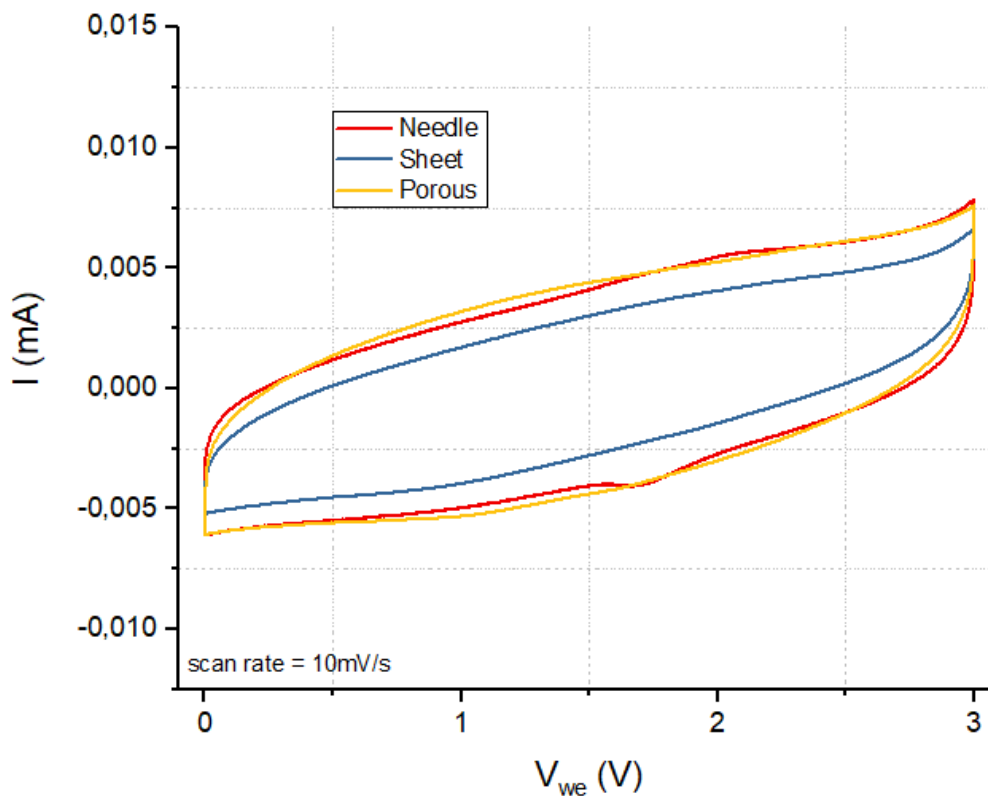


Fig. 4.2 Cyclic Voltammeteries comparison, each morphology CV last cycle

A general evaluation was possible analyzing the voltammetry shape in figure 4.2. The bigger area contained in porous and needle CV curves suggested an higher C_s value respect to the sheet morphology; moreover, the similar slopes indicated comparable device resistance values.

The actual morphologies performance evaluation was done through a galvanostatic measurement with increasing current densities, as previously illustrated. In

picture 4.3 are shown the data concerning specific capacitance and coulombic efficiency with respect to J . The previous C_s assessments about the specific capacitance were reflected in the results: LIG sheet morphology confirmed to be significantly the least capacitive among the three, while the porous one value was slightly less for low current densities, but as J increased the difference became more and more evident. The efficiency analysis found a small difference between the three morphologies, especially at high current densities; η_{Sheet} is marginally above the other two by a few tenths of percentage.

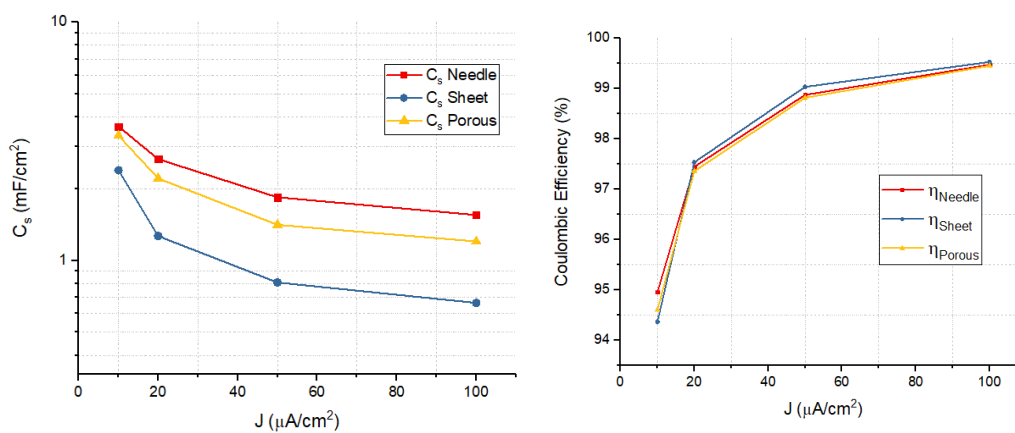


Fig. 4.3 Capacitance and Efficiency behaviour over increasing current density, at 10, 20, 50 and 100 $\mu A/cm^2$

It is possible to observe energy and power densities in a Ragone plot in figure 4.4. The three morphologies performances confirmed the previous C_s results, electing the needle morphology as the best one without doubt. The porous LIG has good electrochemical characteristics and appealing possibilities to graphenise areas instead of simple lines, but the mechanical fragility made the assembly process incredibly difficult, since a minor substrate stress was enough to lead large LIG detachment; the sheet morphology had the worst performance under every aspect, except for coulombic efficiency. One of the leading causes for this behaviour has probably been the high laser scan speed negative influence, since the sheet morphology composition resembled closely the needle one.

The morphology comparison results were quite clear and concluded without doubt that the needle LIG was the best choice, as expected from previous literature work [8]. The reason laying behind can be found in both structure and material composition: the needle-like shape of graphene offers a large and easily accessible

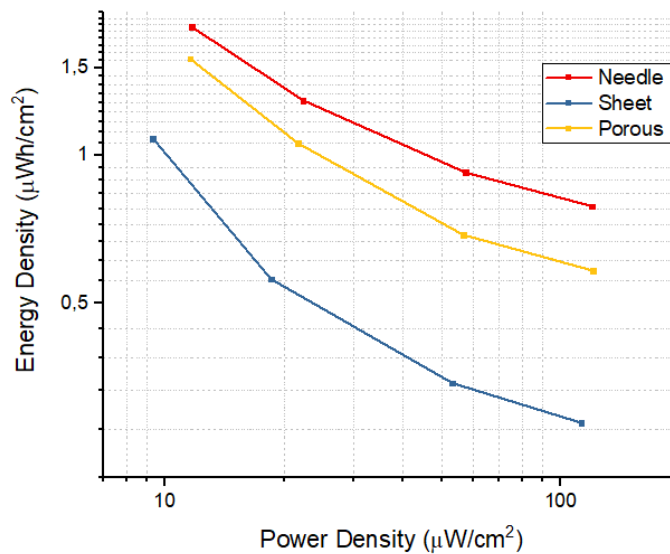


Fig. 4.4 Ragone plots for needle, sheet and porous morphologies

active area, the nitrogen related defects enhance capacitance and the slow laser scan speed positively influences the performance. The further LIG analysis was then performed utilizing just needle morphology samples, which proved to have potential characteristics for optimization processes and for comparing the results with literature.

4.3 Line Writing

The following step in the Laser Induced Graphene implementation concerned the line pattern employed for the electrodes; one of its most appealing characteristics was, in fact, the high degree of design tunability, modifying the laser path on the associated CAD program. For supercapacitor application, the herringbone pattern was chosen for minimizing the distances from one line to the other, and so the ions traveling distance from one electrode to the other. Two different schemes of the same pattern were attempted: a single line one and a double line one, which it is possible to see in figures 4.5 and 4.6. The double line configuration was designed to avoid the laser spot to pass twice in the same point as in the nodes of the monoline geometry, so to reduce the energy transmission to the polymer and lower the structure damages in the critical points.

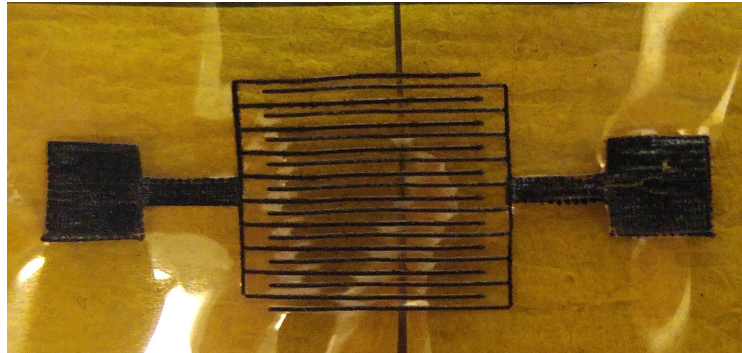


Fig. 4.5 Monoline LIG pattern



Fig. 4.6 Double line LIG pattern

The two typologies reported a similar $LIGArea/Tot.Area$ ratio (~ 0.35) and same electrode distance, in order to focus as much as possible the entire comparison on the sole electrochemical effects. What was found, is that the aspect has little or no effect on a device performance; both the specific capacitance, the power density and the energy density pretty much fit one the other, how it is possible to observe in figure 4.7.

The slight difference between them cannot be addressed to the line pattern, but it rather falls in the randomness range due the production unpredictability. The only double line configuration improvement in the short term was a larger total capacitance, because of the bigger LIG area offered. In order to deepen the analysis between the two patterns, both of them were tested for an high number of charge discharge cycles, in order to test the LIG cyclability and long term differences.

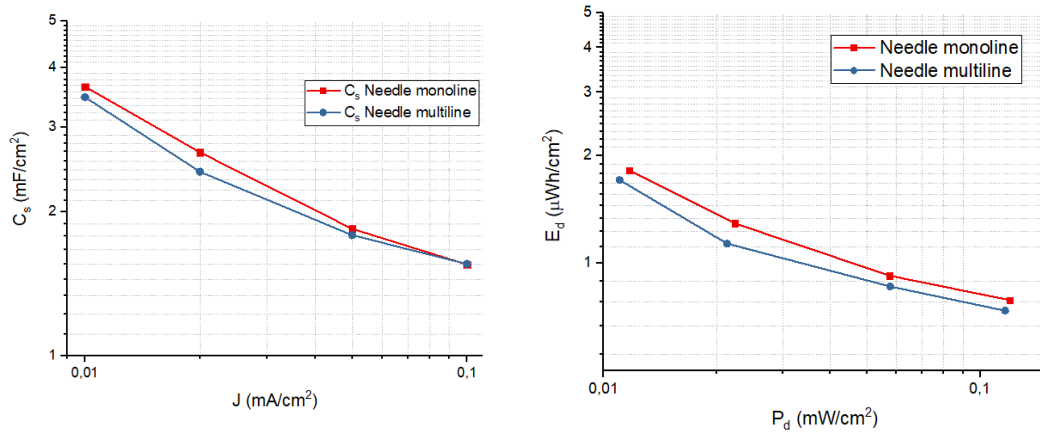


Fig. 4.7 C_s vs Current Density and Ragone plot comparisons for the two line configurations.

4.3.1 Device Cyclability

The devices cycling life was tested performing galvanostatic charges-discharges nonstop for almost two weeks, more than 3000 cycles, with a $20\mu\text{A}/\text{s}$ current density. For both line configurations the specific capacitance and the device efficiency were monitored over time, for evaluating their performance over time. The two devices exploited for the analysis presented non comparable values of specific capacitance, so to avoid any misjudgment they were evaluated in separate graphs in figure 4.8 and 4.9.

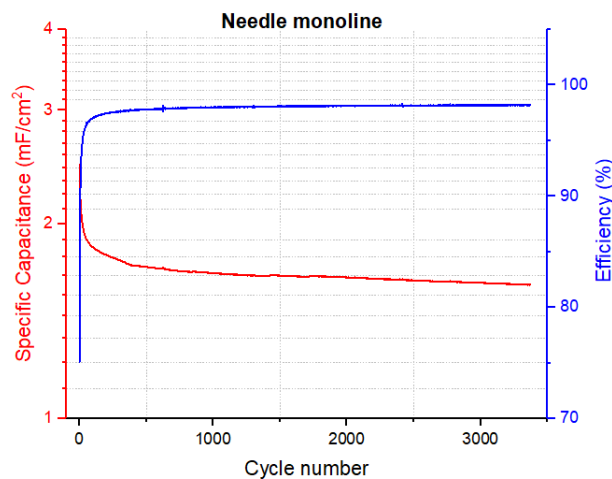


Fig. 4.8 Single line LIG C_s and Efficiency vs number of cycles

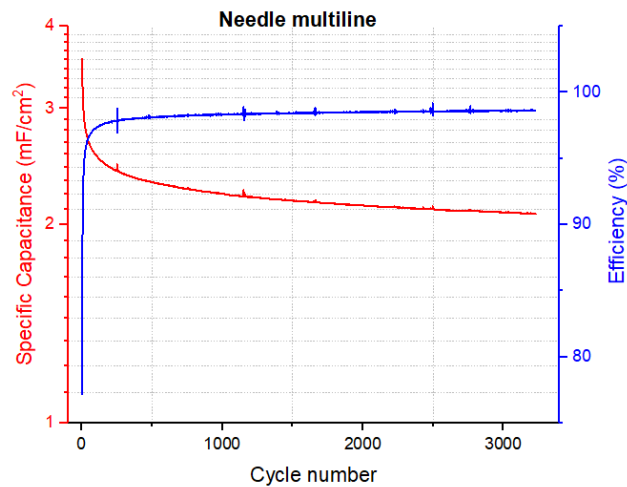


Fig. 4.9 Double line LIG C_s and Efficiency vs number of cycles

In both cases, it is clear that device efficiency did not decrease at all, on the contrary its value raised of a few percentage tenths over time; a clear but not drastic capacitance shrinkage was present, which is possible to evaluate by C_s slope. For further analysis purposes, two single galvanostatic curves from the early and late measurements were compared, for comparing the differences associated to capacitance reduction; the GCD curves are displayed in 4.10. The anode emerged as the main responsible for C_s decrease, an evidence which is shown also graphically: the discharge curve slope is an indicator of the single electrode capacitance, the lower it is the higher the capacitance will be. In this case, the negative electrode showed a quite clear slope increase with respect to the cathode, thus it was pretty straightforward to deduce a major degradation over time on the anode.

In conclusion, the comparison proved that the line pattern choice has a negligible effect on the device performance. Nonetheless, this step was also crucial to confirm the long term cyclability, a desirable characteristic for a supercapacitor; Laser Induced Graphene manifested a high retain in terms of capacitance and coulombic efficiency increase over the cycles, as expected from an EDL supercapacitor, demonstrating then long term stability for potential electronic applications.

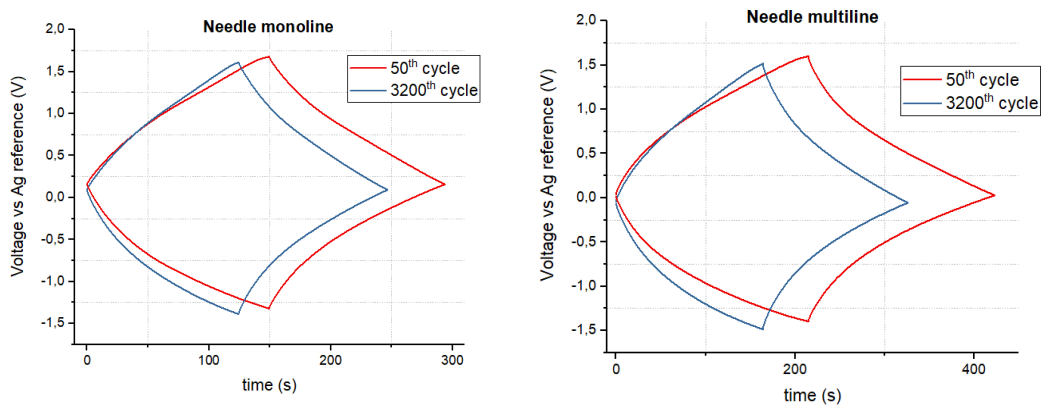


Fig. 4.10 Galvanostatic charge-discharge comparison for the two line configurations, 50th and 3200th

4.4 Literature Comparison

Laser Induced Graphene supercapacitor implementation as electrode material provided positive results, but in order to certify it a comparison with previous literature regarding LIG supercapacitors was required. However, the majority of devices analysed in literature employed aqueous electrolytes, whose characteristics are not comparable with ionic liquids due to lower operating voltage and much higher ion conductivity. The only case of Laser Induced Graphene supercapacitor implementing ionic liquid was found in one of the first scientific articles related to the subject, published by prof. James M. Tour research group (Rice University, Houston, Texas) [13]. In that case, a LIG supercapacitor was assembled using BMIM-BF₄ as electrolyte; as first comparison the specific capacitance were compared, whose graphs are displayed in figure 4.11.

Due to the different current densities employed, the comparison was not straightforward, but there was a common point: the first point in the LIG BMIM-BF₄ plot used the same current density as the last point in the LIG Pyr₁₄TFSI one. The capacitance reported by prof. Tour group is a little higher than the one found in our case, but if the capacitance evaluation formula is taken into account it becomes more than double the value of LIG with Pyr₁₄TFSI, because Rice University research group evaluated the specific capacitance over the whole device active area, not the single electrode one. The main explanation for this considerable difference between results is the different ion conductivity of the two ionic liquids employed; BMIM-BF₄ is less

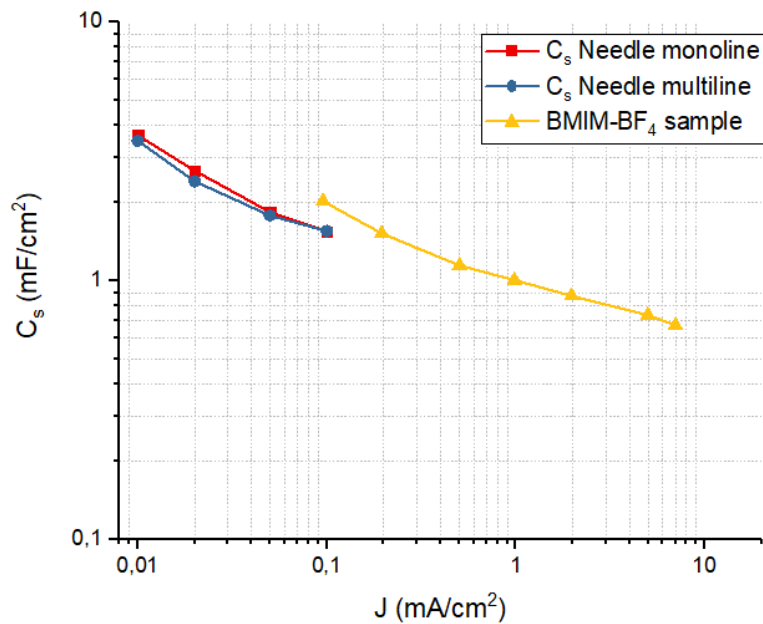


Fig. 4.11 Specific capacitance: the LIG results with Pyr₁₄TFSI compared Tour research group results implementing BMIM-BF₄ at discharge current densities from 0.1 mA/cm⁻² to 7 mA/cm⁻², [13]

viscous and more ion conductive than Pyr₁₄TFSI, their characteristics differences strongly influenced the results.

Another comparison analysis was performed exploiting the Ragone plot present in the same work, in which different energy storage devices performances were reported in the same graph. The needle morphology plot was scaled to match the same axis parameters in the scientific article, in such way it was possible to visualize the collocation of LIG Pyr₁₄TFSI performance with respect to other supercapacitors.

As previously stated, the different ionic liquid strongly influenced the device behaviour: Pyr₁₄TFSI lower ionic conductivity resulted in poorer power density, but on the other hand extending the operating potential boosted the energy density. The reported LIG supercapacitors with aqueous electrolyte had, in fact, E_d values times lower than ionic liquids, due the restricted voltage window often limited to 1 V. Ultimately, the literature comparison led to a positive judgment overall; the ionic liquid implementation translated in higher energy densities as predicted, while the lower ion conductivity represented the biggest drawback.

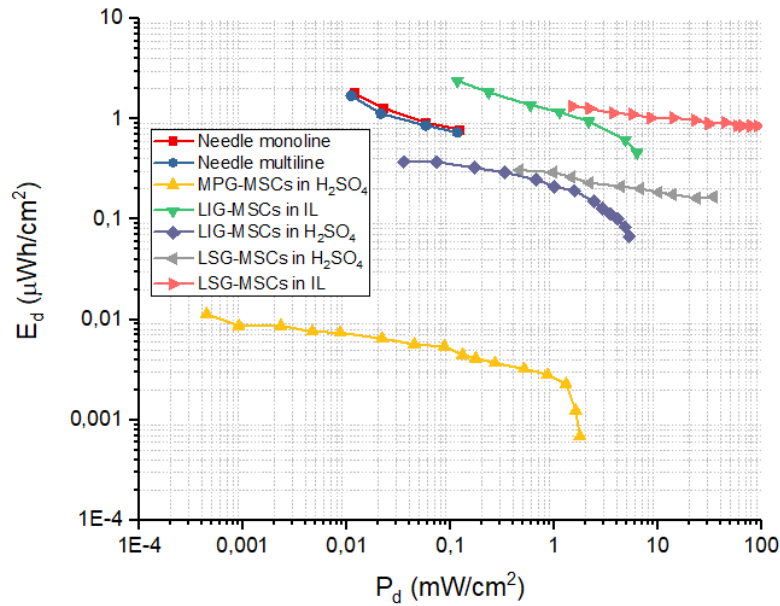


Fig. 4.12 Ragone plot: LIG results with Pyr₁₄TFSI compared to Tour research group data for energy storage devices, [13]

4.5 Optimization Processes

Laser Induced Graphene as electrode material proved to have satisfying performances overall; nevertheless a legitimate question was raised, if some room for improvements was there. To this end some modifications were applied to the assembly process, so to analyse the following results and to compare them with a standard device. Only the monoline needle morphology LIG was employed for the optimization step, since it represented the easiest sample to produce multiple times due its simple pattern.

4.5.1 Interline Tuning

The first parameter analysed was the distance between one electrode line and the other, also called *interline*. Changing it means enlarging or shortening the path ions have to travel from one electrode to the other, which is in the order of hundreds of nanometers. The common sample interline after the lase was ~ 210 nm, in order to examine any influence two other distances were employed, of ~ 310 nm and ~ 410 nm; the enlarging choice was forced by the difficulty to implement any distance lower than 200 nm without shortcircuit risk making the electrodes touch. The three devices

whose characteristics are reported in figures 4.13, 4.14 and 4.15 were selected to have C_s at low current densities as similar as possible, to exclude any misjudgment of interline influence which is really due the values randomness; any effect given by the interline were evaluated from the C_s vs J evolution and the Ragone plot, since a larger ion path might have resulted in a lower power density.

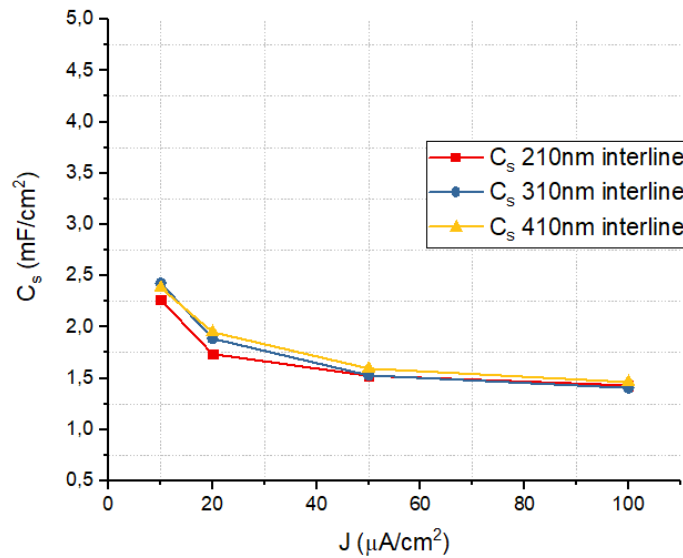


Fig. 4.13 Specific capacitance comparison for different interline values

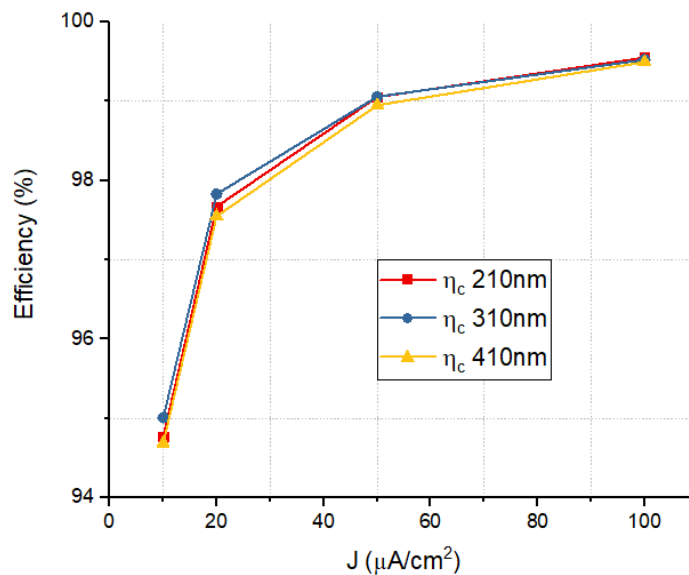


Fig. 4.14 Coulombic efficiency comparison for different interline values

The specific capacitance evolution over increasing current density was almost identical for the three interlines, the small value differences present during the 10 mA/cm^2 GCD disappeared for high current densities. The Ragone plot also confirmed the little effect of interline distance on device performance; the three supercapacitors showed very much alike curves, whose minor difference in terms of energy density could be addressed to production randomness. As further prove of it, there was no linear increase of E_d with the interline: the 310 nm performance was slightly inferior the 210 nm, while the 410 nm one was above the other two. Moreover, as expected the coulombic efficiency was pretty much the same for all three devices.

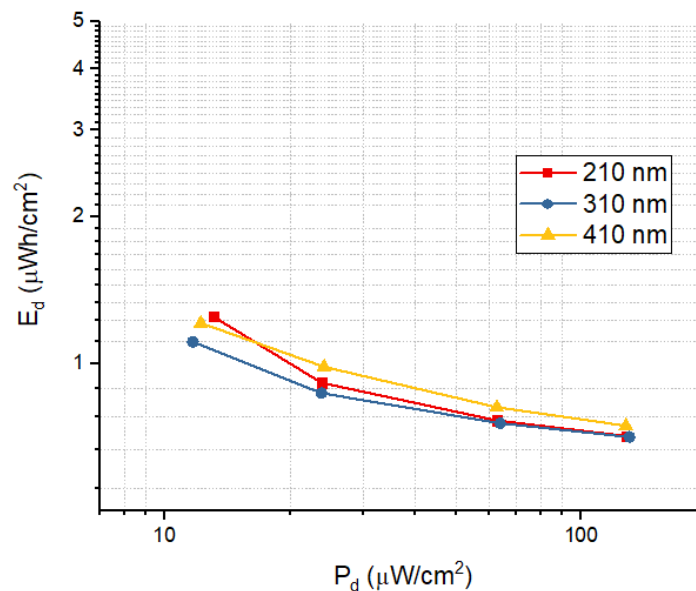


Fig. 4.15 Ragone plots for different interline values

In the end, interline tuning proved to have no effect on the device characteristics; therefore it is reasonable to prefer a lower distance between the electrodes, in such a way to minimize the total area occupied by the LIG supercapacitor on the polyimide surface.

4.5.2 Contact Enhancement

The LIG gas evolution randomness during the lase process affected the interface with the aluminum current collectors, which led to unpredictable resistance values

ranging from hundreds to thousands of Ohms. A better contact resistance would positively affect the performance overall, reason for which a contact enhancement by platinum sputtering was purposed; 30 nm of Pt were sputtered on the contact areas, covering the electrodes with a proper mask. The device was then assembled and tested in comparison to a standard LIG supercapacitor; since the platinum is a noble metal and almost inert, there were no drawbacks as with silver sputtering.

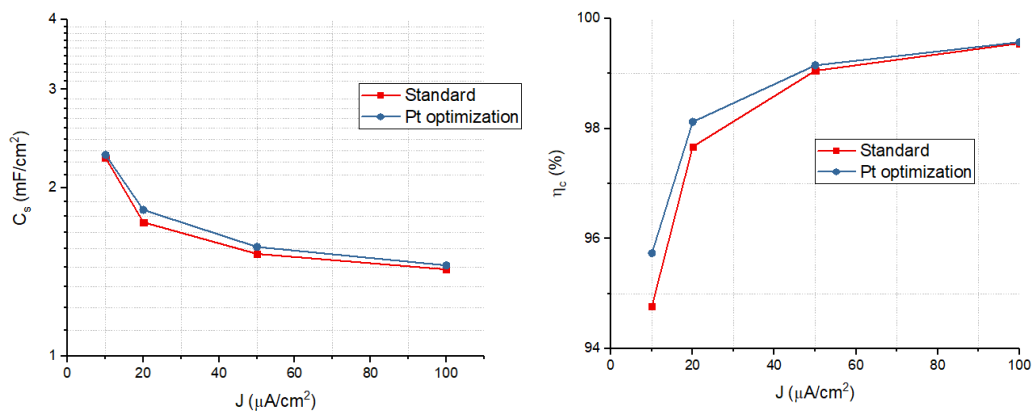


Fig. 4.16 LIG supercapacitor specific capacitance and efficiency, with and without platinum sputtering

In figures 4.16 specific capacitance and coulombic efficiency are analysed. For both of the parameters, platinum sputtering had positive effects: C_s retain was marginally improved from the enhanced contact. Also the coulombic efficiency was bettered of few tenths of percentage at low current densities, while for high J values the difference disappeared. Ragone plot comparison is shown in figure 4.17; as for specific capacitance, with increasing current densities the energy density retain was subjected to improvement, the Pt device showed a much more linear behaviour in comparison to the standard one.

However, the resistance value was not affected at all from the contact enhancement. In figure 4.18 it is possible to see from the Electrochemical Impedance Spectroscopy results that no improvement was made, as matter of fact the LIG device without platinum reported lower impedance values. The contact enhancement process proved to have some minor benefits for Laser Induced Graphene characteristics, but not enough useful if compared to the increased costs for the employment of platinum, which is one of the most expensive materials on the market nowadays.

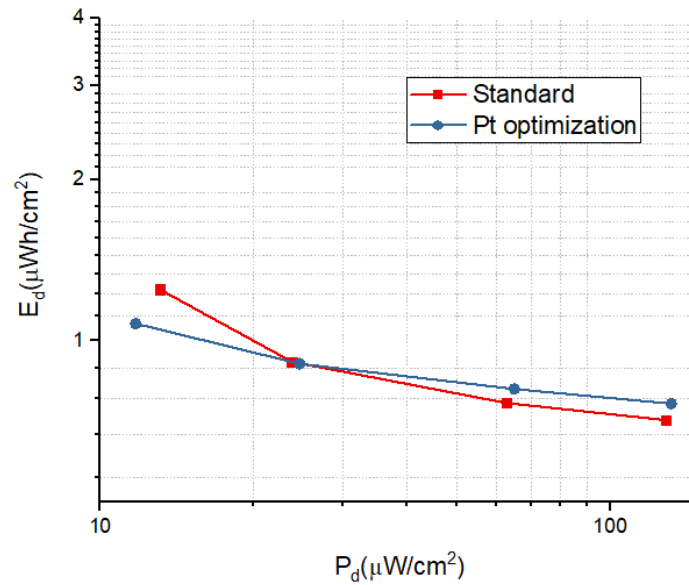


Fig. 4.17 LIG supercapacitor Ragone plots with and without platinum sputtering

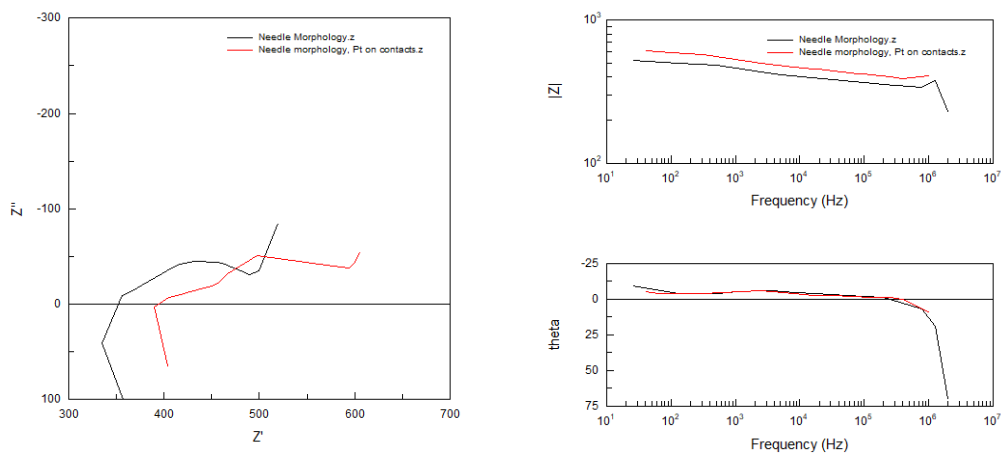


Fig. 4.18 LIG supercapacitor specific EIS, with and without platinum sputtering

4.5.3 LIG Doping

The optimization process exploiting doping focused on two different aspects of Laser Induced Graphene characteristics:

- Nitrogen pseudo-graphene doping with nitric acid, exploiting N-related defects

- Electrode conductivity increasing, through a conductive polymer coating after N-doping

The doping procedure was inspired to previous literature [18], which reported benefits from the treatments in Laser Induced Graphene supercapacitors implementing gel electrolyte; in particular, the nitrogen doping itself proved to affect positively the capacitance, while the combination of N-doping and PEDOT coating resulted in even better capacitance values and lower device resistance, giving the LIG supercapacitor an almost ideal behaviour.

All the LIG samples subjected to this optimization step were treated with nitric acid, then half of them also with PEDOT:PSS coating; the doping process was performed in Turin, inside the DISAT department laboratories. In figures 4.19, 4.20 and 4.21 are shown respectively the specific capacitance vs current density, the coulombic efficiency vs current density and the Ragone plots comparison for the standard device and the doped ones.

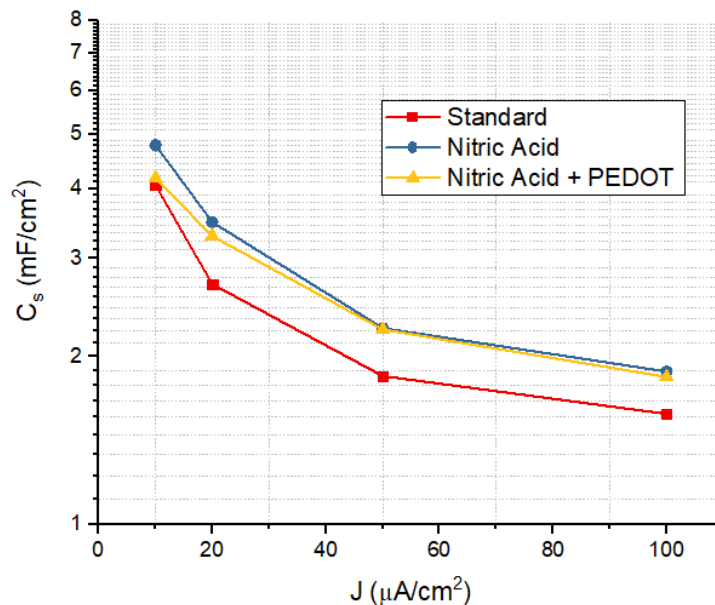


Fig. 4.19 Specific capacitance vs current density of standard LIG and doped LIG devices

From the graphs it is possible to notice how C_s improvement was quite considerable for the doped devices, although not outstanding. The treated-LIG supercapacitors reported a clear capacitance difference from the standard device, especially at high current densities; however, the PEDOT:PSS treatment did not seem to have any

effect at all, since the doped devices curves coincide almost perfectly. The coulombic efficiency instead had a really minor drop, which by the way disappeared for high J values.

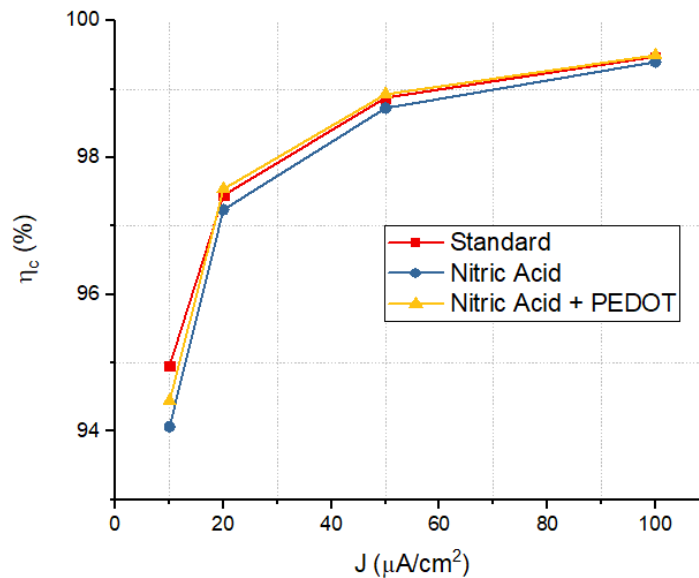


Fig. 4.20 Coulombic efficiency vs current density for standard LIG and doped LIG devices

The doping treatments also reported an improvement in terms of E_d , displayed in the Ragone plots comparison. Surprisingly, the sole nitric acid treatment had a better performance respect the one with PEDOT:PSS afterwards; whilst it might be possible to suppose a degrading effect of the polymer coating on the nitrogen related defects, on the other hand the curves proximity and the C_s data suggested these results to fall in the same broad range of possible values caused by the LIG production system.

To sum up, the characterization of devices implementing treated LIG samples proved doping to have a positive effect for the device performances. Nonetheless, the difference was quite disappointing respect to literature expectations: there were not enough improvements to fully justify the increased complexity and costs, which are added to the process for implementing the optimization step, especially in perspective of an industrial assembly line.

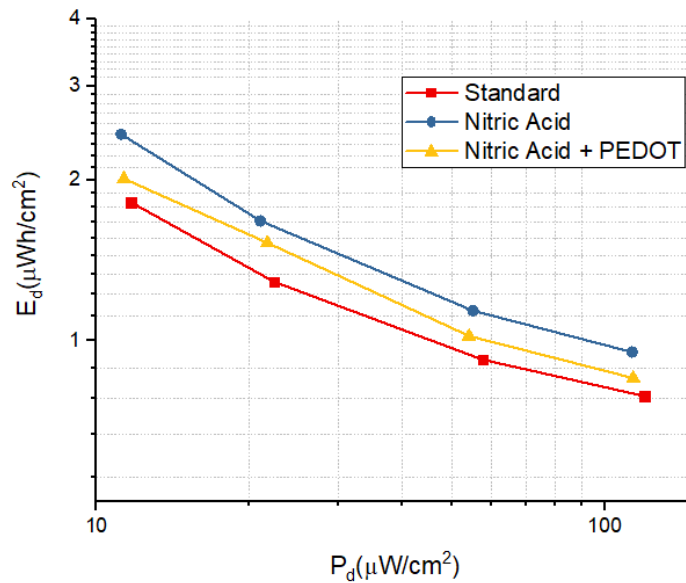


Fig. 4.21 Ragone plots for standard LIG and doped LIG devices

4.5.4 Flexible Assembly

The last attempted optimization focused on the realization of a flexible device, in order to evaluate both the differences as compared to a rigid one and the Laser Induced Graphene bendability. The peculiar characteristic of this process was that no modified nor additional steps were required during the assembly, but rather the removal of two simple steps related to the rigid lab glasses. The first comparison performed was among the standard device and the flexible one.

The flexible supercapacitor reported a clear improvement in terms of specific capacitance retain for increasing current densities, shown in the comparison between them in figure 4.22; the absence of rigid substrates below and above compressed less the structure during the vacuum sealing, leaving intact the LIG porosity. For the same reason, the contact between the aluminum current collector and the electrodes worsened, as proved by the coulombic efficiency drop which is illustrated in figure 4.23. The η_C for low current densities decreased about 1% respect to the standard device, for higher J values the difference decreased but did not disappear.

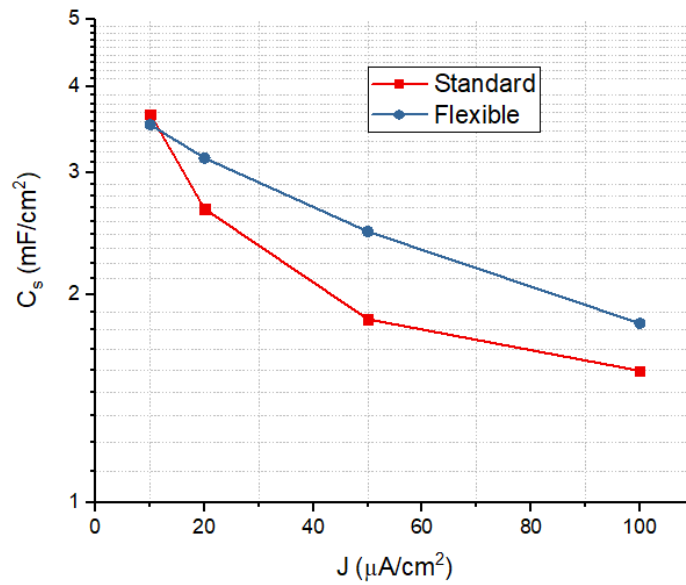


Fig. 4.22 Standard and Flexible supercapacitor C_s vs Current density

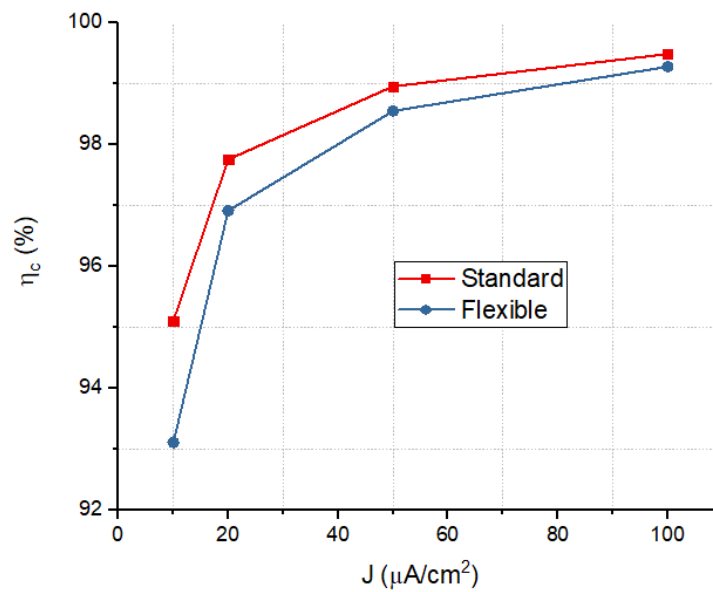


Fig. 4.23 Standard and Flexible supercapacitor Coulombic efficiency against increasing Current density

The flexible device Ragone plot showed a completely different behaviour from the others, which is possible to observe in figure 4.24. The power density for the same current was slightly lower than the standard device, but the energy density

increased noticeably and did not follow the same trend as the previous samples implementing the lab glass.

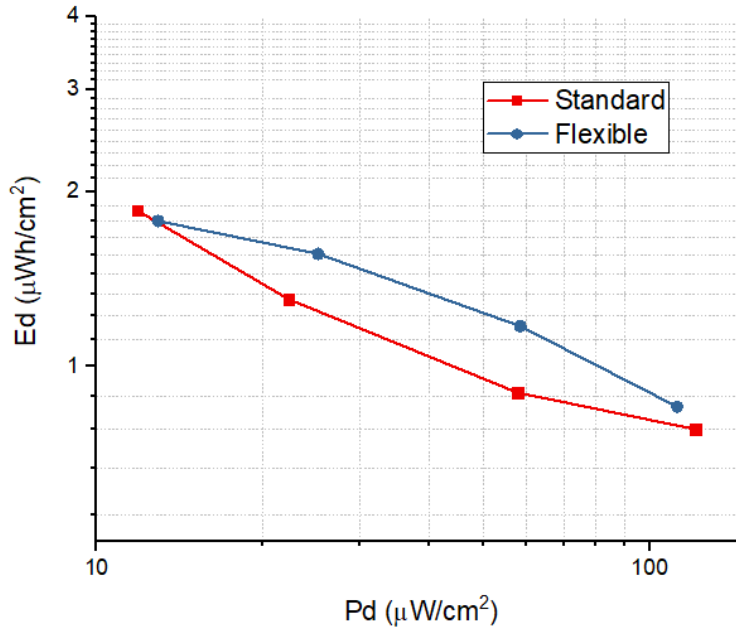


Fig. 4.24 Standard and Flexible supercapacitor Ragone plots, comparison

For the second comparison, the supercapacitor functioning under bending conditions was tested; to do so, two flexible LIG supercapacitors were analysed with two different bending radii, 2 cm for a light bending and 1.25 cm for a hard one. The bent performances were compared with the ones prior to the bending, in order to examine the effects of the mechanical stress on the electrochemical characteristics. In figure 4.25 are reported CV curves for one flexible device before, while and after bending it. The curves different slopes and areas suggested a higher device resistivity and lower capacitance while bending; moreover, the partial process irreversibility was proved: after the bending test, the supercapacitor was made flat again, but the CV curves did not match the ones before bending.

Device bending resulted in a specific capacitance drop which became more critical increasing the bending, as illustrated in figure 4.26. While the decrease was marginal in the case of a 2 cm bending radii, the hard bending severely afflicted C_s , which became half of the original value with high current densities. The coulombic efficiency instead, proved to have some benefits from bending: how it is possible to see in figure 4.27, while no effect is addressed in case of hard bending, the lightly

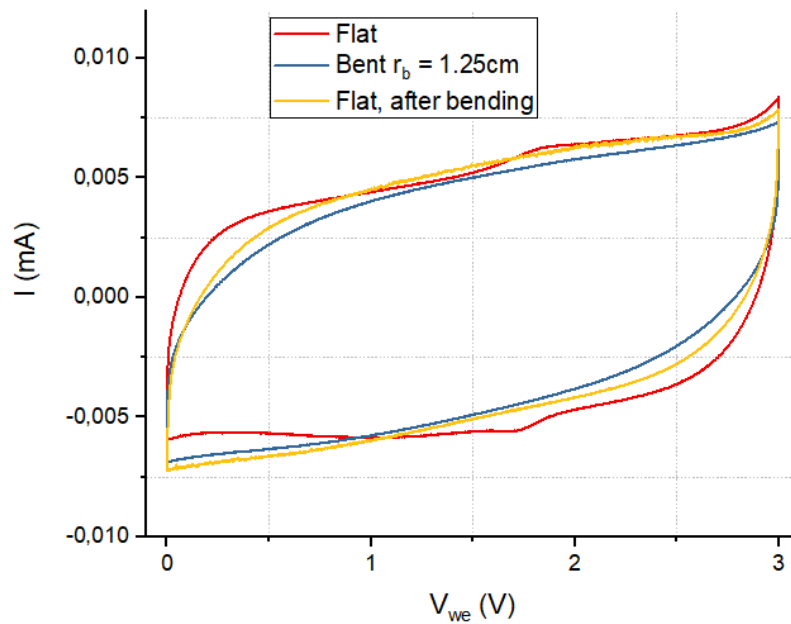


Fig. 4.25 Cyclic Voltammetry comparison for the same device before, during and after the bending process

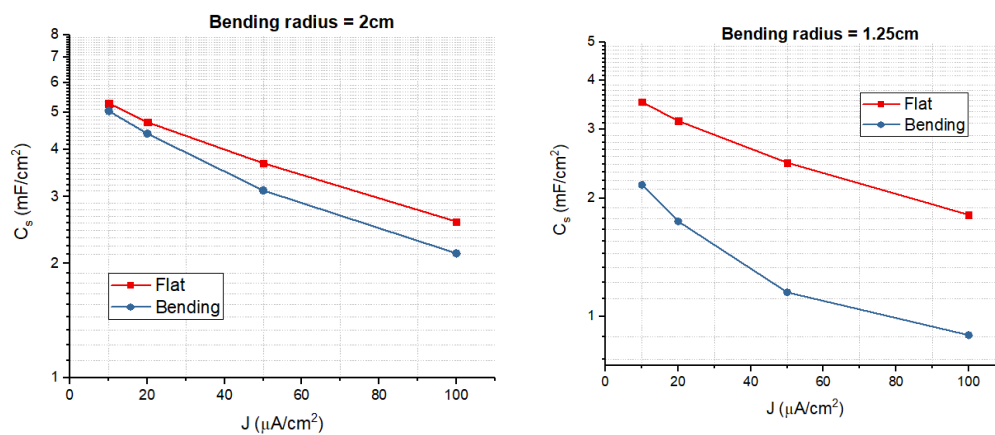


Fig. 4.26 Specific capacitance vs J comparison for the two different bending radii

bent device reported a considerable raise in terms of efficiency, especially at low current densities (almost a 2% increment).

The Ragone plot comparison in two different bending conditions also gave really interesting results. In figure 4.28 the two comparisons are displayed and it is possible to see that, while the light bending simply translated in a performance decrease, the case of 1.25 cm bending radii deeply changed the Ragone plot trend, which

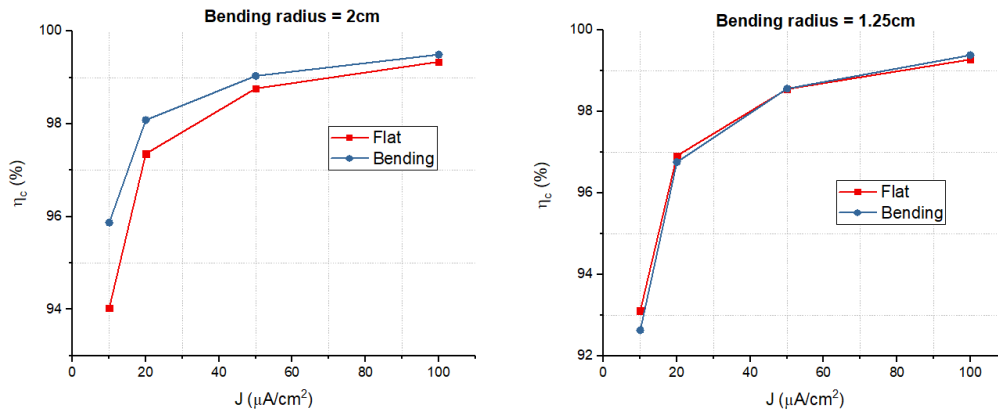


Fig. 4.27 Coulombic efficiency vs J comparison for the two different bending radii

resembled more the standard devices implementing lab glasses. The mechanical stress provided to the material by bending the supercapacitor resembled then the one given in a standard LIG device from the glass pressure.

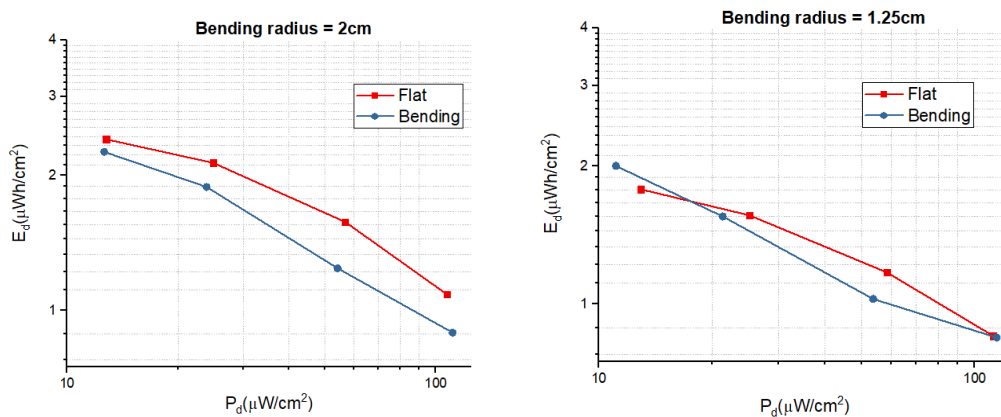


Fig. 4.28 Ragone plots comparison for the two different bending radii

In conclusion, the LIG supercapacitor bendability was proved to be practicable, almost beneficial in some cases. A minor downgrade of the electrochemical characteristics was generally present, nonetheless the possibility to bend an energy storage device represents an incredible advantage and a peculiar feature which has a great potential for future implementation in the flexible electronics field.

4.6 Post Mortem Analysis

The conclusive analysis performed on Laser Induced Graphene supercapacitors was the Post Mortem one, in which the most cycled devices were removed from the vacuum sealed pouches for inspecting the employed LIG electrodes; the devices exploited were needle morphology samples cycled over 3000 times, which were previously discussed during the device cyclability testing. Two were the main objectives of this last process:

- To compare the electrodes structure, morphology and composition before and after thousands of charge-discharge cycles;
- To verify presence or absence of ion intercalation inside the amorphous graphene. Ion intercalation in carbonaceous structures is a well known electrochemical phenomenon [15] [10], which is not desired in EDL supercapacitors since the charge storage mechanism is supposed to be purely electrostatic-based; in particular, the TFSI anion intercalation was monitored.

The examined LIG samples were washed multiple times with ethyl acetate and dried overnight under vacuum, so to remove any trace of $\text{Pyr}_{14}\text{TFSI}$ in the porous structure which would have compromised the results.

4.6.1 XRD

The X-Ray Diffraction data proved the structure to be unquestionably amorphous, with very low and broad peaks; the results plotted in figure 4.29 showed no difference between anode and cathode, as expected from XRD measurement: eventual ion intercalation would have resulted into increased distance between the graphene planes and so broader peaks, but only in an ordered lattice; LIG morphology did not allow to evaluate such a parameter.

The comparison between the pristine electrode and the used ones, instead, pointed out a slight difference between them; the second peak resulted noticeably lower for the worn electrodes, probably because of a slight structure degradation over time.

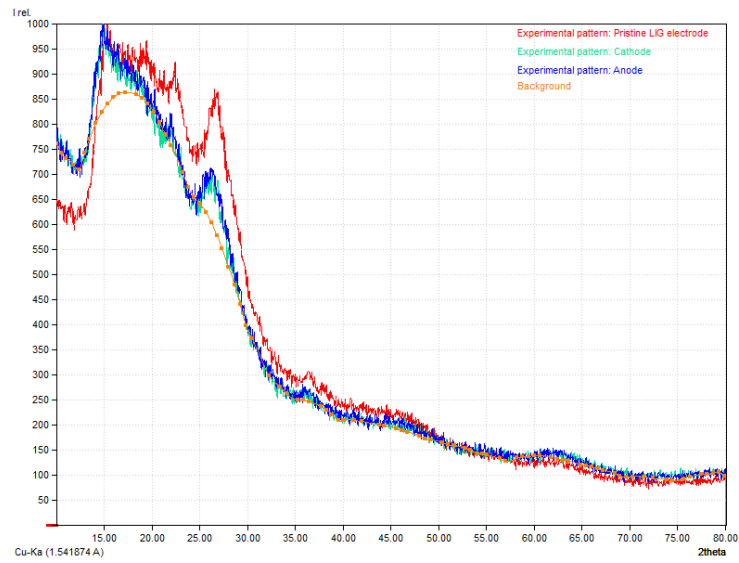


Fig. 4.29 X-Ray Diffraction results for anode, cathode and pristine electrode

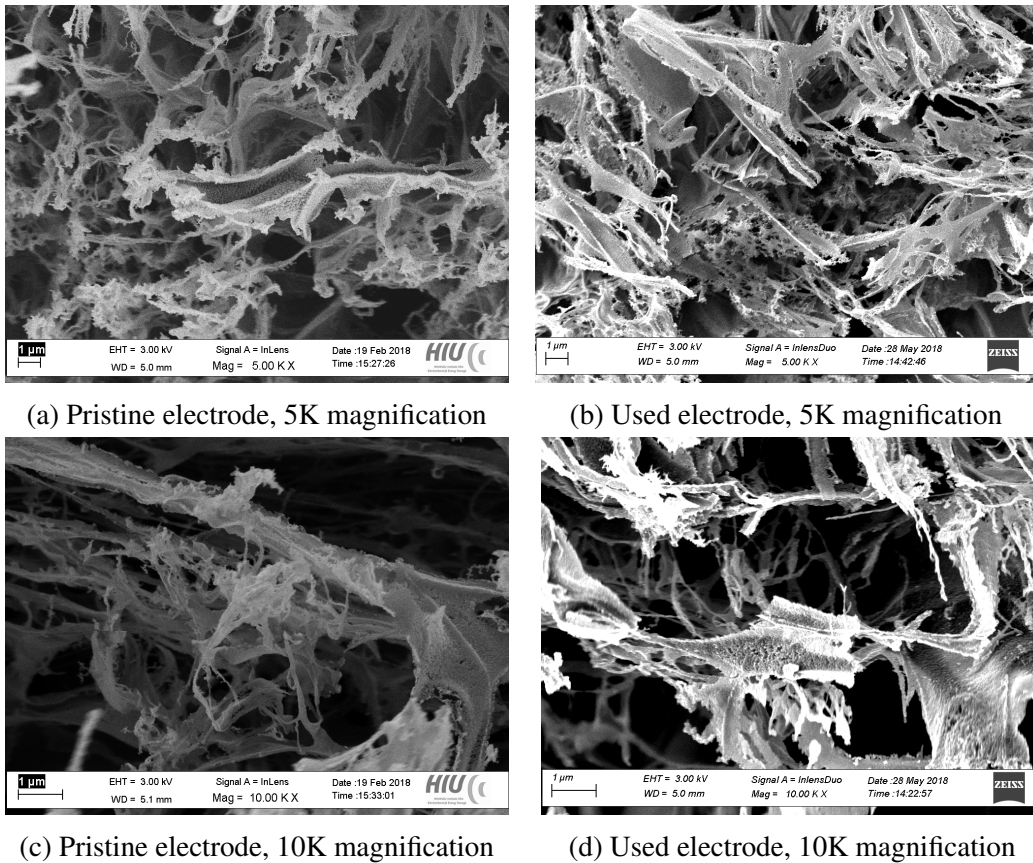


Fig. 4.30 SEM Laser Induced Graphene images at different magnification levels

4.6.2 SEM

Scanning Electron Microscopy examined the morphology of the needle samples before and after their employment, looking for any micrometric exterior difference.

No aspect differences were found in the cycled sample, which appeared indistinguishable from the pristine electrode; the needle morphology shape met the expectation from previous literature [8], the gas evolution granted LIG a fiber structure and impressive active surfaces to exploit for the EDL supercapacitor application. However, after the GCD measurements the focalization process resulted much harder due a serious conductivity decrease, and higher contrast levels were required to have clear shots, as it can be seen in figure 4.30. The lower conductivity may explain partially the performance decrease over time and also have a connection with the XRD results discussed before.

Chapter 5

Conclusions

Convincing results were obtained from the Laser Induced Graphene implementation as supercapacitor electrode, which confirmed the potential of this relatively new material.

The comparison among different morphologies proved the needle one as the best choice over any mechanical and electrochemical aspect; the combination of low frequency and low scan speed for laser writing induce almost monodimensional structure features and nitrogen related defects, which enhance the specific capacitance. The implementation of *Pyr₁₄TFSI* as electrolyte determined inferior performances in terms of specific capacitance and power density if compared to LIG supercapacitors with aqueous electrolytes, due much higher viscosity and much lower volatility; nonetheless in this way an impressive 3V potential window, which resulted in high energy densities. The LIG supercapacitor also proved the long cycle life and good capacitance retain over thousand of cycles, with no effect on the coulombic efficiency.

The optimization processes performed on the device were numerous and suggested that the distance between LIG lines has a marginal role on the electrochemical behaviour, while Pt contact sputtering and LIG doping treatment with nitric acid and PEDOT:PSS gave positive results. However, the improvements obtained were still too low to validate cost and assembly complexity increasing. On the other hand, the flexible LIG supercapacitor resulted a quite interesting and simple optimization to implement, since the flexible devices presented higher capacitance retain and the potential to operate in bending conditions.

Overall, Laser Induced Graphene demonstrated desirable characteristics as electrode and remarkable performances: the optimized LIG samples, in particular the flexible and doped ones, reported specific capacitances higher than 5mF/cm^2 ; energy and power densities for doped devices were reported respectively up to $2.5\mu\text{Wh/cm}^2$ and $125\mu\text{W/cm}^2$.

There are still a lot of improvements which have the potential to further increase LIG appeal as supercapacitor material: new polymeric substrates may be experimented and optimized mechanically and electrochemically; a smaller laser spot respect to today's $300\mu\text{m}$ would allow further interline reduction and more complex patterns; new electrolytes implementation, as for example polymeric ones or diluted ionics liquids.

In conclusion, LIG represents a promising material for applications in electronics and flexible electronics, especially in cases where simple fabrication and low production costs are required

Acknowledgements

I would like to start by thanking the Helmholtz Institute of Ulm, for giving me the opportunity to work with them and for welcoming me since the first day. I am deeply thankful to Dr. Alberto Varzi and Prof. Dr. Stefano Passerini, who constantly helped and supervised me throughout this project, I have learned so much during my seven months in Germany and I could not have done it without them. I also would like to acknowledge some colleagues from HIU who also helped me in some parts which I could not have done by myself, Dr. Varya Sharova for introducing me to the laboratory instrumentation with such patience, Tobias Eisenmann and Yuan Ma for helping me respectively with XRD and SEM measurements and Dr. Sangsik Jeong for the ionic liquid production.

A special mention goes to my supervisor from Politecnico di Torino, Dr. Andrea Lamberti. He made my thesis abroad possible, provided me with so much insight about the subject and gave me many suggestions during the entire period of time; he never put pressure on me and always helped me whenever there was a problem, for these reasons I owe him a lot.

Finally, I would like to finish all my colleagues from Turin and Ulm, for being such a great company during my path, for making both my academic and working environment a wonderful experience, which I will never forget.

References

- [1] AMMRF AUSTRALIAN MICROSCOPY & MICROANALYSIS RESEARCH FACILITY, *Scanning electron microscope*. Training module.
- [2] Y. CHYAN, R. YE, Y. LI, S. P. SINGH, C. J. ARNUSCH, AND J. M. TOUR, *Laser-induced graphene by multiple lasing: Toward electronics on cloth, paper, and food*, ACS Nano, 12 (2018), pp. 2176–2183.
- [3] F. CLERICI, M. FONTANA, S. BIANCO, M. SERRAPEDE, F. PERRUCCI, S. FERRERO, E. TRESSO, AND A. LAMBERTI, *In situ mos2 decoration of laser-induced graphene as flexible supercapacitor electrodes*, Appl. Mater. and Interfaces, 8 (2016), pp. 10459–10465.
- [4] B. E. CONWAY, *Electrochemical Supercapacitors: Scientific Fundamentals and Technological Applications*, Kluwer Academic/Plenum Publishers, 1999.
- [5] G. INSTRUMENTS, *Basics of electrochemical impedance spectroscopy*. Application Note, 2010.
- [6] B. C. KIM, J.-Y. HONG, G. G. WALLACE, AND H. S. PARK, *Recent progress in flexible electrochemical capacitors: Electrode materials, device configuration, and functions*, Adv. Energy Mater., (2015), p. 33.
- [7] B. K. KIM, S. SY, A. YU, AND J. ZHANG, *Electrochemical supercapacitors for energy storage and conversion*, Handbook of Clean Energy Systems, (2018), p. 25.
- [8] A. LAMBERTI, , F. PERRUCCI, M. CAPRIOLI, M. SERRAPEDE, M. FONTANA, S. BIANCO, S. FERRERO, AND E. TRESSO, *New insights on laser-induced graphene electrodes for flexible supercapacitors: tunable morphology and physical properties*, Nanotechnology, 28 (2017), p. 9.
- [9] A. LAMBERTI, M. SERRAPEDE, G. FERRARO, M. FONTANA, F. PERRUCCI, S. BIANCO, A. CHIOLERIO, AND S. BOCCHINI, *All-speak flexible supercapacitor exploiting laser-induced graphenization*, 2D Mater, 4 (2017), p. 10.
- [10] T. LEILEI, Z. QUANCHAO, L. JIA, S. YUELI, C. JIANPENG, L. FENG1, AND S. SHIGANG, *Mechanism of intercalation and deintercalation of lithium ions in graphene nanosheets*, Chinese Sci Bull, 56 (2011), pp. 3204–3211.

- [11] L. LI, J. ZHANG, Z. PENG, Y. LI, C. GAO, Y. JI, R. YE, N. D. KIM, Q. ZHONG, Y. YANG, H. FEI, G. RUAN, AND J. M. TOUR, *High-performance pseudocapacitive microsupercapacitors from laser-induced graphene*, *Adv. Mater.*, 28 (2016), p. 838–845.
- [12] Y. LI, D. X. LUONG, J. ZHANG, Y. R. TARKUNDE, C. KITTRELL, F. SARGUNARAJ, Y. JI, C. J. ARNUSCH, AND J. M. TOUR, *Laser-induced graphene in controlled atmospheres: From superhydrophilic to superhydrophobic surfaces*, *Adv. Mater.*, 29 (2017), p. 8.
- [13] J. LIN, Z. PENG, Y. LIU, F. RUIZ-ZEPEDA, R. YE, E. L. SAMUEL, M. J. YACAMAN, B. I. YAKOBSON, AND J. M. TOUR, *Laser-induced porous graphene films from commercial polymers*, *NATURE COMMUNICATIONS*, 5 (2014), p. 8.
- [14] Z. PENG, J. LIN, R. YE, E. L. G. SAMUEL, AND J. M. TOUR, *Flexible and stackable laser-induced graphene supercapacitors*, *Appl. Mater. Interfaces*, 7 (2015), pp. 3414–3419.
- [15] X. QI, B. BLIZANAC, A. DUPASQUIER, P. MEISTER, T. PLACKE, M. OLJACA, J. LI, AND M. WINTER, *Investigation of pf_6^- and $tfsi^-$ anion intercalation into graphitized carbon blacks and its influence on high voltage lithium ion batteries*, *The Royal Society of Chemistry*, (2013), p. 8.
- [16] F. SHI, L. LI, X. LI WANG, C. DONG GU, AND J. PING TU, *Metal oxide/hydroxide-based materials for supercapacitors*, *RSC Advances*, 4 (2014), pp. 41910–41921.
- [17] D. A. SOKOLOV, K. R. SHEPPERD, AND T. M. ORLANDO, *Formation of graphene features from direct laser-induced reduction of graphite oxide*, *J. Phys. Chem. Lett.*, 1 (2010), pp. 2633–2636.
- [18] W. SONG, J. ZHU, B. GAN, S. ZHAO, H. WANG, C. LI, AND J. WANG, *Flexible, stretchable, and transparent planar microsupercapacitors based on 3d porous laser-induced graphene*, *Small*, 14 (2018), p. 7.
- [19] J. TARASCON AND M. ARMAND, *Issues and challenges facing rechargeable lithium batteries*, *Nature*, 414 (2001), pp. 359–367.
- [20] M. WINTER AND R. J. BRODD, *What are batteries, fuel cells and supercapacitors*, *Chem. Rev.*, 104 (2004), pp. 4245–4269.
- [21] R. YE, Y. CHYAN, J. ZHANG, Y. LI, X. HAN, C. KITTRELL, AND J. M. TOUR, *Laser-induced graphene formation on wood*, *Adv. Mater.*, 29 (2017), p. 7.
- [22] S. ZHANG AND N. PAN, *Supercapacitors performance evaluation*, *Adv. Energy Mater.*, 5 (2015), p. 19.

-
- [23] M. ZHI, C. XIANG, J. LI, M. LI, AND N. WU, *Nanostructured carbon–metal oxide composite electrodes for supercapacitors: a review*, *Nanoscale*, 5 (2013), pp. 72–88.
- [24] C. ZHONG, Y. DENG, W. HU, J. QIAO, L. ZHANG, AND J. ZHANG, *A review of electrolyte materials and compositions for electrochemical supercapacitors*, *Chem. Soc. Rev.*, 44 (2015), pp. 7484–7539.
- [25] C. ZHONG, Y. DENG, W. HU, D. SUN, X. HAN, J. QIAO, AND J. ZHANG, *Electrolytes for Electrochemical Supercapacitors*, Taylor & Francis Group, 2016.